THE ASTROPHYSICAL JOURNAL, 544:302–319, 2000 November 20
© 2000. The American Astronomical Society. All rights reserved. Printed in U.S.A.

NEUTRON-CAPTURE ELEMENTS IN THE EARLY GALAXY: INSIGHTS FROM A LARGE SAMPLE OF METAL-POOR GIANTS

DEBRA L. BURRIS,[1] CATHERINE A. PILACHOWSKI,[2] TAFT E. ARMANDROFF,[2] CHRISTOPHER SNEDEN,[3] JOHN J. COWAN,[4] AND HENRY ROE[5]

Received 1999 August 2; accepted 2000 June 27

ABSTRACT

New abundances for neutron-capture (*n*-capture) elements in a large sample of metal-poor giants from the Bond survey are presented. The spectra were acquired with the KPNO 4 m echelle and coudé feed spectrographs, and have been analyzed using LTE fine-analysis techniques with both line analysis and spectral synthesis. Abundances of eight *n*-capture elements (Sr, Y, Zr, Ba, La, Nd, Eu, and Dy) in 43 stars have been derived from blue ($\lambda\lambda$4070–4710, $R \sim 20{,}000$, S/N ratio $\sim$ 100–200) echelle spectra and red ($\lambda\lambda$6100–6180, $R \sim 22{,}000$, S/N ratio $\sim$ 100–200) coudé spectra, and the abundance of Ba only has been derived from the red spectra for an additional 27 stars.

Overall, the abundances show clear evidence for a large star-to-star dispersion in the heavy element-to-iron ratios. This condition must have arisen from individual nucleosynthetic events in rapidly evolving halo progenitors that injected newly manufactured *n*-capture elements into an inhomogeneous early Galactic halo interstellar medium. The new data also confirm that at metallicities [Fe/H] $\lesssim -2.4$, the abundance pattern of the heavy ($Z \geq 56$) *n*-capture elements in most giants is well-matched to a scaled solar system *r*-process nucleosynthesis pattern.

The onset of the main *r*-process can be seen at [Fe/H] ≈ -2.9; this onset is consistent with the suggestion that low mass Type II supernovae are responsible for the *r*-process. Contributions from the *s*-process can first be seen in some stars with metallicities as low as [Fe/H] ~ -2.75 and are present in most stars with metallicities [Fe/H] > -2.3. The appearance of *s*-process contributions as metallicity increases presumably reflects the longer stellar evolutionary timescale of the (low-mass) *s*-process nucleosynthesis sites.

The lighter *n*-capture elements (Sr-Y-Zr) are enhanced relative to the heavier *r*-process element abundances. Their production cannot be attributed solely to any combination of the solar system *r*- and main *s*-processes, but requires a mixture of material from the *r*-process and from an additional *n*-capture process that can operate at early Galactic time. This additional process could be the weak *s*-process in massive ($\sim 25\ M_\odot$) stars, or perhaps a second *r*-process site, i.e., different from the site that produces the heavier ($Z \geq 56$) *n*-capture elements.

Subject headings: galaxies: evolution — nuclear reactions, nucleosynthesis, abundances — stars: abundances — stars: Population II

1. INTRODUCTION

The oldest metal-poor halo stars are Galactic fossils that provide clues to the conditions and populations of stars that existed early in the Galaxy's history. The chemical compositions of these halo stars are due to only a few, perhaps one, earlier generations of stars. Metal-poor stars provide an opportunity to observe neutron-capture (*n*-capture) elements ($Z > 30$) produced in the unseen precursors to Population II, and, through their abundances, to deduce characteristics of the first Galactic stellar population.

The *n*-capture elements are produced through both slow (*s*-) and rapid (*r*-) *n*-capture processes. The *s*- and *r*-processes are believed to occur at different sites. The *r*-process requires a high neutron flux level (with many *n*-captures over a timescale of a fraction of a second) thought to occur in supernova explosions, while the *s*-process, which requires a lower neutron flux (with a typical *n*-capture taking many years), is generally thought to occur during the double-shell burning phase of low (1–3 $M_\odot$) and intermediate-mass (4–7 $M_\odot$) asymptotic giant branch (AGB) stars. In the solar system, where the abundances of individual isotopes can be determined (Anders & Ebihara 1982; Anders & Grevesse 1989; Käppeler et al. 1989; Wisshak, Voss, & Käppeler. 1996), the relative fractions of elements produced by each process can be identified (see Sneden et al. 1996, and Appendix).

The production mechanisms for *n*-capture elements in metal-poor stars have been the subject of some debate in the literature. Many observational and theoretical studies (Spite & Spite 1978; Truran 1981; Sneden & Parthasarathy 1983; Sneden & Pilachowski 1985; Gilroy et al. 1988; Gratton & Sneden 1991, 1994; Sneden et al. 1994; McWilliam et al. 1995a, 1995b; Cowan et al. 1996; Sneden et al. 1996; Ryan, Norris, & Beers 1996) have demonstrated that the observed abundances of *n*-capture elements in metal-poor stars are consistent with production via the *r*-process, and, at least for the heaviest such elements, correspond to

[1] Oklahoma City Community College, Division of Science and Mathematics, 7777 S. May Avenue, Oklahoma City, OK 73159; dburris@okc.cc.ok.us.

[2] NOAO, PO Box 26732, Tucson, AZ 85726-6732. The National Optical Astronomy Observatories (NOAO) is operated by the Association of Universities for Research in Astronomy, Inc. (AURA) under cooperative agreement with the National Science Foundation; caty@noao.edu, armand@noao.edu.

[3] Department of Astronomy and McDonald Observatory, University of Texas, Austin, TX 78712; chris@verdi.as.utexas.edu.

[4] Department of Physics and Astronomy, University of Oklahoma, Norman, OK 73019; cowan@mail.nhn.ou.edu.

[5] University of California at Berkeley, Berkeley, CA 94720; hroe@doty.berkeley.edu.

the scaled solar system *r*-process signature (Gilroy et al. 1988; Cowan et al. 1995, 1997, 1999; Sneden et al. 1996, 1998). Gilroy et al. was one of the first large surveys of these metal-poor stars, and confirmed the operation of the *r*-process at low metallicity. Gilroy et al. also revealed significant star-to-star scatter in the overall abundance level of the *n*-capture elements with respect to iron for stars with [Fe/H] < -2.0[6].

The surveys of Beers, Preston, & Shectman (1985, 1992) increased manyfold the number of observed ultra–metal-poor stars (i.e. [Fe/H] < -3), extending the range of metallicity over which *n*-capture element abundance patterns can be investigated. Spectroscopy of a sample of 33 ultra–metal-poor stars by McWilliam et al. (1995a, 1995b) confirmed the large star-to-star scatter in the [*n*-capture/Fe] abundance ratios at low metallicity. An extreme example is the *n*-capture–rich, ultra–metal-poor ([Fe/H] $\simeq -3.1$) star CS 22892−052 (McWilliam et al. 1995a, 1995b; Sneden et al. 1994). Cowan et al. (1995) showed that this star's observed *n*-capture element abundances display the detailed signature of the scaled solar system *r*-process abundances. The case became even more compelling when abundances were determined for additional *n*-capture elements, including several elements (terbium, holmium, thulium, and hafnium) that had never before been detected in metal-poor halo stars (Sneden et al. 1996).

Other studies (see Magain 1995; François 1996; Mashonkina, Gehren, Bikmaev 1999) have found the case for an r-process origin of the *n*-capture elements to be less certain. Since the dispersion in *n*-capture element abundances compared to iron is so large for stars with metallicities below [Fe/H] < -1.0, much of the disagreement can be traced to the small number and particular selection of stars included. Even with the Gilroy et al. (1988) and McWilliam et al. (1995a, 1995b) surveys, the number of metal-poor stars with well-determined *n*-capture abundances remains small, particularly in the metallicity regime $-2.5 <$ [Fe/H] < -1.0. (Edvardsson et al. 1993, Woolf, Tomkin, & Lambert 1995, and Jehin et al. 1999 surveyed numerous stars with metallicities [Fe/H] > -1.0.) The metallicity range $-3.0 <$ [Fe/H] < -1.5 covers a critical transition during which *s*-process elements begin to appear in the Galactic chemical mix. Fortunately, the Bond (1980, hereafter Bond giants) survey of metal-poor giants provides a sample of relatively bright stars in the appropriate metallicity range to investigate this transition and to delineate the history of enrichment of *n*-capture elements in the Galaxy.

In the present paper, we present *n*-capture element abundances (specifically Sr, Y, Zr, Ba, La, Nd, Eu, and Dy) for 43 metal-poor Bond giants, and Ba abundances only for an additional 27 Bond giants on a uniform system of metallicity. In § 2 we present observational data and in § 3 the analysis of the abundances. In § 4 we discuss the observed abundances in the context of nucleosynthesis and Galactic chemical enrichment, and in § 5 we summarize our conclusions.

2. OBSERVATIONS AND REDUCTIONS

Observations of 43 Bond giants were obtained with the Kitt Peak National Observatory 4 m Mayall Telescope during observing runs in 1998 November and 1989 June. The spectrograph was configured with the 31.6 l mm^{-1} echelle grating, a 226 l mm^{-1} cross dispersing grating blazed at 8500 Å, and the UV fast camera (0.267 m focal length). A $CuSO_4$ filter isolated the second order of the cross disperser. The detectors, 800 × 800 pixel Texas Instruments CCDs designated "TI2" or "TI3," were binned two pixels in the spatial direction to reduce the effect of readout noise. The spectra were aligned nearly parallel to the columns of the CCD to facilitate the extraction of one-dimensional spectra. The stars observed are sufficiently bright that sky subtraction was not needed. The gratings were oriented to provide complete spectral coverage from λ4070 to λ4710 in 18 overlapping orders. Exposure times ranged from 1800 s for the brighter stars to 7200 s for the fainter ones.

Calibration data include 20 bias and 20 flat-field frames taken each night, as well as an overscan region on each CCD frame. Data reductions followed standard IRAF[7] procedures. Each set of calibration frames was combined to remove cosmic-ray events and to reduce the noise. For each data image, the bias level determined from the overscan region and the corrected, average bias frame were subtracted. The image was then divided by the bias-corrected, combined, normalized, flat-field frame. The IRAF task *apscatter* was used to subtract scattered light in each echelle image, and the one-dimensional spectra were extracted. A list of stellar lines whose wavelengths are well determined in the solar spectrum was used to determine the wavelength calibration, and the continua were normalized to unity. Spectra of a Th-Ar comparison lamp were also obtained at the beginning and end of each night. The resolving power of the spectra, measured from the FWHM (0.23 Å) of the Th-Ar lines near 4600 Å is $R \sim 20{,}000$. The S/N ratio per pixel varies from a few hundred (typically 200) in the orders at the red end of the spectrum to about 100 in the orders at the blue end.

The same 43 giants, as well as 27 additional Bond giants, were also observed using the coudé feed telescope and spectrograph to obtain spectra of the red λ6141 Ba II feature. Because the stars are red and the gratings and detectors have greater efficiency in the red, we were able to use the smaller (0.9 m) telescope for these observations. Spectra were obtained in 1988 November and in 1989 May. The spectrograph was configured with the large collimator, the 632 l mm^{-1} "A" grating, camera 5 (1.08 m focal length), and the "TI3" detector. Exposure times ranged from a few minutes for the brightest stars to 2 hours for fainter stars. Calibration procedures were similar to those described for the 4 m echelle observations. The resolving power is slightly higher, $R \sim 22{,}000$, from measured Th-Ar line FWHM of 0.28 Å. The S/N ratio is typically between 100 and 200 per pixel.

3. ABUNDANCE DETERMINATIONS

The abundance analyses were performed with the LTE spectral line analysis code MOOG (Sneden 1973), adopting the model atmospheres of Pilachowski, Sneden, & Kraft

[6] We adopt the usual spectroscopic notations that $[A/B] \equiv \log_{10}(N_A/N_B)_{star} - \log_{10}(N_A/N_B)_\odot$, and that $\log \epsilon(A) \equiv \log_{10}(N_A/N_H) + 12.0$, for elements A and B. Also, metallicity will be arbitrarily defined here to be equivalent to the stellar [Fe/H] value.

[7] IRAF is distributed by the National Optical Astronomy Observatories, which are operated by the Association of Universities for Research in Astronomy, Inc., under cooperative agreement with the National Science Foundation.

(1996, hereafter PSK) for most stars. Those models were computed with the atmosphere code of Gustafsson et al. (1975). PSK adopted effective temperatures ($T_{\rm eff}$) from calibrations of $V-R$ and Strömgren $b-y$ photometric indices. The gravity (log g) was computed from the mean of up to three independent estimates: from the star's absolute magnitude (as deduced from its Strömgren c_1 index); from its implied position in the M92 color-magnitude diagram; and from an average $T_{\rm eff}$ versus log g relationship for metal-poor giants gleaned from other studies in the literature. The microturbulent velocity (v_t) was estimated from a correlation of $T_{\rm eff}$ and (v_t) values for metal-poor giants, except that for horizontal branch stars, a uniform value of $v_t = 1.8$ km s^{-1} was adopted. In a few cases, PSK made small adjustments to the $T_{\rm eff}$, log g, and v_t parameters through abundance computations from their line data. See PSK for a more complete description of the derivation of model atmosphere parameters for our stars. For stars not included by PSK, models were adopted as noted in Table 1. A new model atmosphere was generated for HD 29574 in an attempt to improve the fit of the Ti and Fe spectral features from the models of PSK (see below).

The final model atmospheric parameters adopted for each star are listed in Table 1, where [M/H] is the metallicity with respect to the Sun of the models used in the analysis. Abundance uncertainties due to errors in the model atmospheres and atmospheric parameters were discussed in more detail in Sneden et al. (1996).

The atomic transitions used in the analysis and the atomic line data were adopted primarily from the extensive work of Sneden et al. (1996). Our choice of *n*-capture elements was somewhat restricted, being limited by the observed wavelength ranges ($4070 < \lambda < 4710$ Å, and $6100 < \lambda < 6141$ Å), and by the intrinsic weakness of most *n*-capture element transitions in low-metallicity stars. No spectral features in the range from $\lambda\lambda$4225–4280 were included because of the contamination from CH *G*-band features in some stars. Furthermore, since our chief goal was to trace the evolution of *n*-capture elements as a function of stellar metallicity, we included only elements that appear in our spectra over a wide range of [Fe/H]. Thus we did not include some elements (e.g., Sm and Ce, which do appear in more metal-rich stars) because they become undetectable in lower metallicity stars at our resolution and S/N ratio. The lines included in our analysis and references to the atomic data are listed in Table 2.

Before deriving abundances of the *n*-capture elements, we determined abundances of Ti and Fe from up to 10 transitions of singly ionized species in the $\lambda\lambda$4450–4700 region of our blue echelle spectra. Our purpose was to establish whether the PSK model atmospheres employed with our echelle spectra here yield metallicities in reasonable agreement with the PSK results, with particular attention to the adopted microturbulence values, which PSK could not determine from their spectra. In Figure 1 we correlate abundances derived from the newly measured Fe II and Ti II lines with $[{\rm Fe/H}]_{\rm PSK}$ and $[{\rm Ca\ I/H}]_{\rm PSK}$. The iron abundances compared in the top panel are in excellent accord: $\langle\delta[{\rm Fe/H}]\rangle = +0.06 \pm 0.02$ ($\sigma = 0.16$; 43 stars), in the sense Fe II *minus* $\rm Fe_{PSK}$, with no trend with metallicity. Overall, these abundance correlations confirm that the PSK models and atmospheric parameters are suitable for use with the echelle spectra considered here, and provide reliable abundances. With the exceptions noted below, the microturbulence values adopted from PSK were confirmed by our Fe II and Ti II equivalent widths.

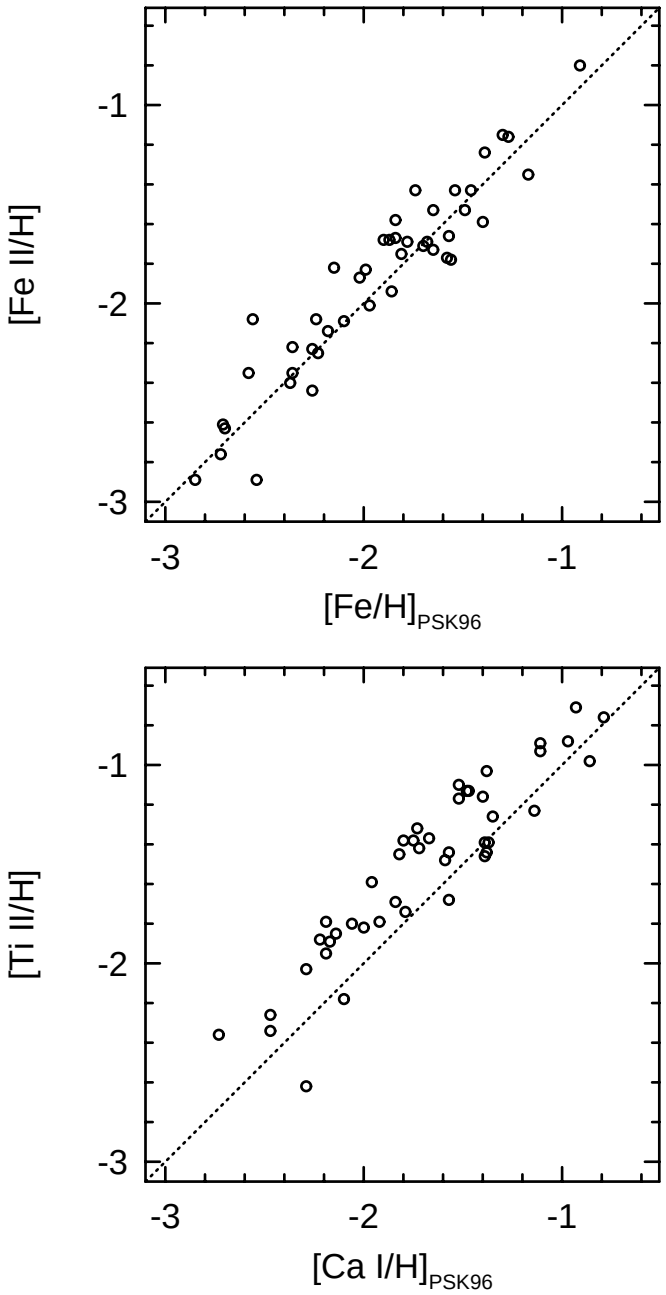

FIG. 1.—*Top panel:* comparison of iron abundance from this work with PSK. *Bottom panel:* comparison of [Ti/H] with [Ca/H] from PSK.

Our [Ti/Fe] overabundances are, however, somewhat larger than are those of [Ca/Fe] from PSK: $\langle([{\rm Ti\ II/H}]-[{\rm Fe/H}]_{\rm PSK96})\rangle = +0.45 \pm 0.03$ ($\sigma = 0.20$), as compared with $\langle([{\rm Ca\ I/H}]-[{\rm Fe/H}]_{\rm PSK96})\rangle = +0.23 \pm 0.02$, ($\sigma = 0.12$). The Ti II lines in many of our more metal-rich and cooler stars are quite strong, much more so than are the Fe II lines. For most of our stars the mean Ti II equivalent widths were greater than 100 mÅ, and the strongest of these lines often exceeded 180 mÅ. Thus they lie on the flat part of the curve of growth, and abundances derived from them are sensitive to choices of v_t. Such very strong lines might not be reproduced very well by our model atmospheres and adopted analysis procedures. For the nine program stars

TABLE 1

MODEL ATMOSPHERE PARAMETERS

Star	Model[a]	$T_{\rm eff}$ (K)	log g	[M/H]	v_t (km s^{-1})	Note
HD 20	PSK	5475	2.80	−1.20	2.00	...
HD 97	PSK	5025	2.60	−1.20	1.20	1
HD 2665	PSK	5000	2.20	−3.00	1.30	...
HD 2796	PSK	4900	1.60	−3.00	1.60	...
HD 3008	PSK	4150	0.60	−2.00	2.20	1, 2
HD 3179	(PSK)	5300	2.60	−0.80	1.90	1
HD 4306	PSK	4900	2.00	−3.00	1.40	1
HD 6268	PSK	4700	1.60	−3.00	1.60	...
HD 6755	PSK	5150	2.70	−1.50	1.40	...
HD 8724	PSK	4500	1.20	−2.20	1.60	...
HD 13979	PSK	5075	1.90	−3.00	1.30	...
HD 25532	PSK	5300	1.90	−1.20	2.30	...
HD 26297	PSK	4400	1.10	−1.70	2.00	...
HD 29574	new	4250	0.00	−1.65	1.90	...
HD 44007	PSK	4850	2.00	−1.50	1.50	...
HD 63791	PSK	4725	1.70	−1.50	1.60	...
HD 74462	PSK	4600	1.50	−1.40	1.80	...
HD 83212	PSK	4550	1.50	−1.20	1.80	1, 2
HD 85773	PSK	4450	1.10	−2.00	2.10	...
HD 88609	PSK	4575	1.40	−3.00	1.80	1, 2
HD 93529	PSK	4650	1.70	−1.50	1.40	1
HD 103545	PSK	4725	1.70	−3.00	1.30	1
HD 104893	PSK	4500	1.10	−2.20	1.90	1
HD 105546	PSK	5300	2.50	−1.00	1.50	...
HD 107752	PSB	4700	1.70	−3.00	1.40	1
HD 108317	PSK	5300	2.90	−2.20	1.00	1, 2
HD 108577	PSK	4975	1.70	−1.50	1.90	1
HD 110184	PSK	4250	0.30	−2.20	2.10	...
HD 115444	PSK	4750	1.70	−3.00	1.60	1, 2
HD 121135	PSK	4925	1.50	−1.50	2.00	1
HD 122563	PSK	4625	1.40	−3.00	1.70	...
HD 122956	PSK	4600	1.50	−1.70	1.80	...
HD 126587	McW	4910	1.85	−3.00	2.00	...
HD 128279	PSK	5275	2.80	−2.00	1.00	1, 2
HD 135148	PSK	4275	0.80	−1.70	2.10	...
HD 165195	PSK	4450	1.10	−2.00	1.90	...
HD 166161	PSK	5150	2.20	−1.00	2.00	...
HD 171496	PSK	4700	1.60	−1.00	1.50	...
HD 175305	PSK	5100	2.50	−1.50	1.40	...
HD 186478	PSK	4575	1.40	−2.20	2.00	...
HD 187111	PSK	4250	0.70	−1.70	1.70	...
HD 204543	PSK	4700	1.70	−1.50	2.00	...
HD 206739	PSK	4675	1.70	−1.70	1.70	...
HD 214362	PSK	5650	1.50	−1.70	1.80	1
HD 216143	PSK	4525	0.80	−2.00	1.80	...
HD 218857	PSK	5125	2.40	−2.00	1.20	...
HD 220838	PSK	4450	1.20	−1.70	1.90	...
HD 221170	PSK	4425	1.00	−2.00	1.50	...
HD 232078	PSK	4000	0.30	−1.50	2.60	...
CD −24°1782.....	PSB	5300	2.80	−2.20	1.50	...
CD −23°72	PSK	5300	2.60	−1.00	2.00	1
BD −18°5550.....	PSK	4575	1.40	−3.00	1.80	1, 2
BD −15°5781.....	PSK	4750	1.20	−3.00	1.70	1
BD −11°145	(PSK)	4800	1.70	−2.00	1.60	1
BD −3°5215	PSK	5700	2.80	−1.20	1.80	1, 2
BD −1°2582	PSK	5150	2.50	−2.00	1.20	1
BD +1°2916	PSK	4150	0.10	−1.80	2.30	...
BD +3°2782	SKPL91	4600	1.50	−2.00	1.80	1
BD +4°2466	(PSK)	5000	1.00	−1.80	1.30	1
BD +6°648	PSK	4500	1.10	−2.00	2.00	...
BD +9°2870	PSK	4600	1.40	−2.20	1.70	...
BD +9°3223	PSK	5350	2.00	−2.20	2.00	...
BD +11°2998.....	PSK	5425	2.30	−1.20	2.20	...
BD +17°3248.....	PSK	5250	2.30	−1.80	1.50	...

TABLE 1—*Continued*

Star	Model[a]	$T_{\rm eff}$ (K)	log g	[M/H]	v_t (km s^{-1})	Note
BD +18°2757.....	PSK	4850	1.50	−1.40	1.90	1
BD +18°2890.....	PSK	5000	2.20	−1.40	1.30	1
BD +30°2611.....	PSK	4275	0.80	−1.40	2.10	...
BD +52°1601.....	PSK	4750	1.60	−1.50	2.00	1
BD +54°1323.....	PSK	5300	2.50	−1.50	1.70	...
BD +58°1218.....	PSK	5000	2.20	−3.00	1.00	...

NOTE—1. Abundances derived from red Ba II λ6141 spectra only. 2. Eu abundances derived from equivalent widths from Gilroy et al. (1988).

[a] Model parameters have been derived as follows: PSK—Pilachowski, Sneden, & Kraft 1996; (PSK)—models have been derived following the methodology of PSK; new—model parameters from PSK have been revised to obtain a better fit to the Fe and Ti equivalent widths; McW—McWilliam et al. 1995a; SKPL91—Sneden et al. 1991; PSB—Pilachowski et al. 1993.

with the weakest Ti II equivalent widths ($\lesssim$130 mÅ), $\langle$([Ti II/H]–[Fe/H]$_{\rm PSK96}$)$\rangle$ = +0.26, in much better agreement with the $\langle$([Ca I/H]–[Fe/H]$_{\rm PSK96}$)$\rangle$ from the whole sample.

The majority of the *n*-capture transitions that we used are blended with other features; therefore, we chose to perform spectral syntheses rather than to determine the abundances from single-line, equivalent-width analysis. Figure 2 shows examples of the synthetic spectra for HD 63791. The lines were fitted by synthesizing spectra with a range of element/iron ratios, typically ranging from one-tenth solar to three times solar, then adjusting the element/iron ratios to bracket the best fit. With two exceptions, we were able to derive the *n*-capture element abundances from at least two detected lines. In HD 232078 and BD +30°2611, spectra of the λ4077 Å region were not usable owing to low S/N ratio and line blending. In these two stars, the Sr and Dy abundances are from single lines. For the unblended lines Nd II λ4446 and λ4462 we were able to employ equivalent width analysis. These lines were measured with the equivalent width subroutine of the SPECTRE code (Fitzpatrick & Sneden 1987), and the abundances were determined directly by MOOG. These abundances were then averaged with the synthesis abundances obtained for the Nd II λ4358 and λ4109 lines to obtain a final Nd abundance.

The elements Ba, La, and Eu must be given special attention, since they are subject to isotopic and/or hyperfine splitting that can affect the final abundances. These effects were treated in the same fashion as in Sneden et al. (1996). Fortunately, abundances derived from the Ba II λ6141 line are not as sensitive to the distribution of Ba isotopes, which differ depending on whether the barium is produced by the *r*-process or the *s*-process. But even for the λ4554 line, the assumption of a different isotopic distribution can change the derived abundance by up to only ∼0.1 dex when the feature is strong.

The Ba abundance is also sensitive to the microturbulent velocity because it is derived from strong lines, with equivalent widths ≥60 mÅ (most other lines used in this analysis are typically weak). Several of the stars showed a difference between the Ba abundance derived from the λ4554 and the λ6141 features, in the sense that the abundance derived from the λ4554 line was a few tenths of a dex larger than

TABLE 2

ATOMIC DATA FOR LINES USED

Species	λ (Å)	χ (eV)	log (gf)	References
Sr II.....	4077.71	0.00	+0.17	1
	4215.52	0.00	−0.17	1
Y II	4358.73	0.10	−1.32	2
	4398.01	0.13	−1.00	2
Zr II	4161.21	0.71	−0.72	3
	4317.32	0.71	−1.38	3
Ba II	4554.03	0.00	+0.17	4
	6141.73	0.70	−0.07	4
La II	4086.71	0.00	−0.16	1
	4123.23	0.32	+0.12	1
	4333.76	0.17	−0.16	1
Nd II[a].....	4109.46	0.32	+0.18	5
	4358.16	0.32	−0.12	5
	4446.39	0.20	−0.63	6
	4462.99	0.56	−0.07	6
Eu II	4129.70	0.00	+0.204	7
	4205.05	0.00	+0.117	7
Dy II.....	4103.31	0.10	−0.37	8
	4077.96	0.10	−0.01	8

[a] Oscillator strengths for Nd II lines have been adjusted as described by Sneden et al. (1996).

REFERENCES—(1) Gratton & Sneden 1994; (2) Hannaford et al. 1982; (3) Biémont et al. 1981; (4) Gallagher 1967; (5) Maier & Whaling 1977; (6) Ward et al. 1984, 1985 modified; (7) Biémont et al. 1982; (8) Kusz 1992, Biémont & Lowe 1993.

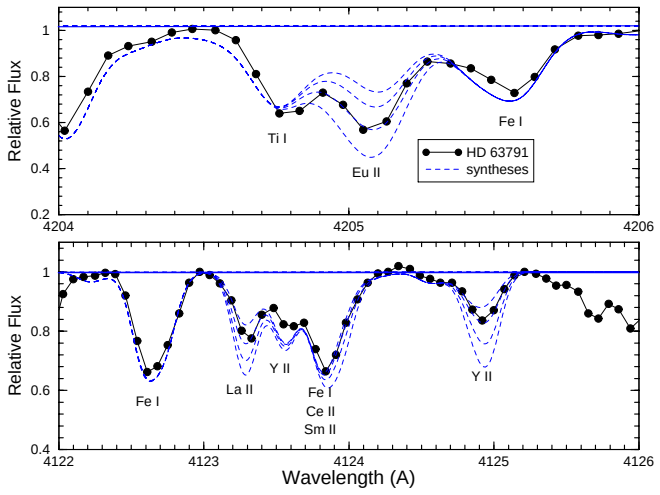

FIG. 2.—Spectrum synthesis for (*lower panel*) the La 4123 Å and (*upper panel*) Eu 4205 Å lines for HD 63791.

TABLE 3

HEAVY ELEMENT ABUNDANCES ([M/Fe]) IN METAL-POOR STARS

Star	[Fe/H]	[Sr/Fe]	[Y/Fe]	[Zr/Fe]	[Ba/Fe]	[La/Fe]	[Nd/Fe]	[Eu/Fe]	[Dy/Fe]
HD 20	−1.39	0.05	−0.05	0.46	0.58	0.39	0.58	0.77	0.92
HD 97	−1.19	...	...	...	0.50	...	...	...	...
HD 2665	−1.97	−0.45	−0.39	−0.20	−0.05	−0.19	0.22	0.23	0.28
HD 2796	−2.23	0.13	−0.39	−0.07	−0.16	−0.22	−0.24	−0.06	0.03
HD 3008	−1.93	...	...	...	0.08	...	...	0.77	...
HD 3179	−1.04	...	...	...	0.39	...	...	...	...
HD 4306	−2.54	...	...	...	−1.09	...	...	...	...
HD 6268	−2.36	0.08	−0.18	0.32	0.50	0.21	0.39	0.52	0.68
HD 6755	−1.57	−0.08	−0.26	0.07	0.15	0.09	0.42	0.50	0.52
HD 8724	−1.84	0.04	−0.25	−0.06	−0.01	−0.07	0.07	0.20	0.47
HD 13979	−2.26	−0.07	−0.63	−0.34	−0.50	−0.10	−0.40	−0.38	−0.10
HD 25532	−1.46	0.14	−0.28	0.14	0.17	−0.07	0.00	0.10	0.26
HD 26297	−1.87	...	−0.12	0.06	−0.26	−0.21	0.14	0.11	0.37
HD 29574	−1.81	...	−0.24	0.59	0.59	0.38	0.16	0.76	...
HD 44007	−1.70	0.20	0.36	0.22	0.05	−0.20	0.46	0.19	0.22
HD 63791	−1.68	0.06	−0.10	0.06	0.05	−0.21	0.15	0.12	0.23
HD 74462	−1.56	−0.09	−0.14	0.02	−0.06	−0.06	0.41	0.32	0.49
HD 83212	−1.43	...	...	...	0.40	...	...	0.51	...
HD 85773	−2.36	...	−0.31	0.07	−0.49	0.09	0.19	0.24	0.48
HD 88609	−2.93	...	...	...	−0.70	...	...	−0.33	...
HD 93529	−1.67	...	...	...	0.25	...	...	...	...
HD 103545	−2.14	...	...	...	−0.04	...	...	...	...
HD 104893	−1.97	...	...	...	0.08	...	...	...	...
HD 105546	−1.27	0.45	0.13	0.45	0.42	0.05	0.30	0.32	0.19
HD 107752	−2.69	...	...	...	−0.24	...	...	...	...
HD 108317	−2.24	...	...	...	0.58	...	...	0.71	...
HD 108577	−2.28	...	...	...	0.00	...	...	...	...
HD 110184	−2.56	...	0.46	1.13	0.01	0.11	0.29	0.45	...
HD 115444	−2.77	...	...	...	−0.05	...	...	0.65	...
HD 121135	−1.57	...	...	...	0.20	...	...	...	...
HD 122563	−2.71	0.06	−0.13	0.31	−0.92	−0.71	−0.59	−0.30	−0.39
HD 122956	−1.78	0.18	−0.18	0.16	0.15	0.04	0.43	0.55	0.60
HD 126587	−2.85	−0.45	0.01	0.50	−0.06	0.30	0.75	0.75	0.65
HD 128279	−2.00	...	...	...	−0.59	...	...	−0.08	...
HD 135148	−1.90	...	0.88	0.50	0.30	0.27	1.07	0.58	...
HD 165195	−2.24	...	−0.18	0.42	0.23	0.19	0.35	0.58	0.57
HD 166161	−1.30	0.20	0.31	0.43	0.53	0.36	0.33	0.10	0.23
HD 171496	−0.91	0.06	−0.13	−0.26	−0.07	−0.47	0.15	−0.15	0.10
HD 175305	−1.40	0.13	−0.11	0.10	0.12	0.05	0.34	0.44	0.40
HD 186478	−2.58	0.38	−0.01	0.40	0.23	−0.04	0.30	0.57	0.68
HD 187111	−1.74	...	−0.25	0.52	0.10	0.06	0.09	0.36	...
HD 204543	−1.84	0.00	−0.12	0.20	0.36	0.27	0.59	0.46	0.79
HD 206739	−1.58	0.10	0.00	0.00	0.05	−0.17	0.24	0.35	0.48
HD 214362	−1.90	...	...	...	0.47	...	...	...	...
HD 216143	−2.18	0.33	−0.17	0.13	0.03	0.06	0.30	0.43	0.63
HD 218857	−1.86	0.01	−0.17	0.00	0.03	−0.36	−0.06	−0.23	0.16
HD 220838	−1.65	...	−0.03	0.10	0.11	−0.20	0.41	0.30	0.50
HD 221170	−2.15	...	−0.14	0.35	0.50	0.50	0.75	0.80	0.85
HD 232078	−1.54	...	−0.10	0.34	0.06	0.12	0.69	0.40	...
CD −24°1782	−2.70	−0.10	0.24	0.50	−0.38	0.33	0.60	<0.49	<0.35
CD −23°72	−1.17	...	...	...	0.34	...	...	...	...
BD −18°5550	−2.93	...	...	...	−0.90	...	...	−0.07	...
BD −15°5781	−2.36	...	...	...	−0.57	...	...	...	...
BD −11°145	−2.28	...	...	...	0.25	...	...	...	...
BD −3°5215	−1.16	...	...	...	0.46	...	...	0.56	...
BD −1°2582	−2.25	...	...	...	1.50	...	...	...	...
BD +1°2916	−1.99	...	−0.07	0.64	0.07	0.35	0.42	0.65	...
BD +3°2782	−2.03	...	...	...	0.03	...	...	...	...
BD +4°2466	−2.00	...	...	...	1.60	...	...	...	...
BD +6°648	−2.10	0.35	−0.03	0.33	0.15	0.13	0.34	0.29	0.40
BD +9°2870	−2.37	−0.20	−0.25	0.05	−0.46	−0.53	−0.40	−0.25	−0.23
BD +9°3223	−2.26	0.16	0.00	0.44	0.41	0.20	0.17	0.42	0.35
BD +11°2998	−1.17	−0.20	−0.23	0.17	0.14	−0.17	−0.10	0.06	−0.05
BD +17°3248	−2.02	0.55	0.06	0.50	0.97	0.60	0.88	0.96	0.96
BD +18°2757	−2.19	...	...	...	0.35	...	...	...	...
BD +18°2890	−1.58	...	...	...	0.26	...	...	...	...
BD +30°2611	−1.49	...	−0.20	0.04	0.08	0.15	0.77	0.45	...
BD +52°1601	−1.58	...	...	...	0.15	...	...	...	...
BD +54°1323	−1.65	0.57	−0.14	0.20	0.37	0.11	0.29	0.47	0.65
BD +58°1218	−2.72	0.17	−0.10	0.06	−0.50	−0.30	0.03	0.21	0.37

TABLE 4

HEAVY ELEMENT ABUNDANCES [log ϵ(m)] IN METAL-POOR STARS

Star	[Fe/H]	log ϵ(Sr)	log ϵ(Y)	log ϵ(Zr)	log ϵ(Ba)	log ϵ(La)	log ϵ(Nd)	log ϵ(Eu)	log ϵ(Dy)
HD 20	−1.39	1.56	0.80	1.67	1.32	0.22	0.69	−0.11	0.63
HD 97	−1.19	...	...	...	1.44	...	...	...	...
HD 2665	−1.97	0.48	−0.12	0.43	0.11	−0.94	−0.25	−1.23	−0.59
HD 2796	−2.23	0.80	−0.38	0.30	−0.26	−1.23	−0.97	−1.78	−1.10
HD 3008	−1.93	...	...	...	0.28	...	...	−0.65	...
HD 3179	−1.04	...	...	...	1.48	...	...	...	...
HD 4306	−2.54	...	...	...	−1.50	...	...	...	...
HD 6268	−2.36	0.62	−0.30	0.56	0.27	−0.93	−0.47	−1.33	−0.58
HD 6755	−1.57	1.25	0.41	1.10	0.71	−0.26	0.35	−0.56	0.05
HD 8724	−1.84	1.10	0.15	0.70	0.28	−0.69	−0.27	−1.13	−0.27
HD 13979	−2.26	0.57	−0.65	0.00	−0.63	−1.14	−1.16	−2.13	−1.26
HD 25532	−1.46	1.58	0.50	1.28	0.84	−0.31	0.04	−0.85	−0.10
HD 26297	−1.87	...	0.25	0.79	0.00	−0.86	−0.23	−1.25	−0.40
HD 29574	−1.81	...	0.19	1.38	0.91	−0.21	−0.15	−0.54	...
HD 44007	−1.70	1.40	0.90	1.12	0.48	−0.68	0.26	−1.00	−0.38
HD 63791	−1.68	1.28	0.46	0.98	0.50	−0.67	−0.03	−1.05	−0.35
HD 74462	−1.56	1.25	0.54	1.06	0.51	−0.40	0.35	−0.73	0.03
HD 83212	−1.43	...	...	...	1.10	...	...	−0.41	...
HD 85773	−2.36	...	−0.43	0.31	−0.72	−1.05	−0.67	−1.61	−0.78
HD 88609	−2.93	...	...	...	−1.50	...	...	−2.75	...
HD 93529	−1.67	...	...	...	0.71	...	...	...	...
HD 103545	−2.14	...	...	...	−0.05	...	...	...	...
HD 104893	−1.97	...	...	...	0.24	...	...	...	...
HD 105546	−1.27	2.08	1.10	1.78	1.28	0.00	0.53	−0.44	0.02
HD 107752	−2.69	...	...	...	−0.80	...	...	...	...
HD 108317	−2.24	...	...	...	0.47	...	...	−1.02	...
HD 108577	−2.28	...	...	...	−0.15	...	...	...	...
HD 110184	−2.56	...	0.14	1.17	−0.42	−1.23	−0.77	−1.60	...
HD 115444	−2.77	...	...	...	−0.69	...	...	−1.61	...
HD 121135	−1.57	...	...	...	0.76	...	...	...	...
HD 122563	−2.71	0.25	−0.60	0.20	−1.50	−2.20	−1.80	−2.50	−2.00
HD 122956	−1.78	1.30	0.28	0.98	0.50	−0.52	0.15	−0.72	−0.08
HD 126587	−2.85	−0.40	−0.60	0.25	−0.78	−1.33	−0.60	−1.59	−1.10
HD 128279	−2.00	...	...	...	−0.46	...	...	−1.57	...
HD 135148	−1.90	...	1.22	1.20	0.53	−0.41	0.67	−0.81	...
HD 165195	−2.24	...	−0.18	0.78	0.12	−0.83	−0.39	−1.15	−0.57
HD 166161	−1.30	1.80	1.25	1.73	1.36	0.28	0.53	−0.69	0.03
HD 171496	−0.91	2.05	1.20	1.43	1.15	−0.16	0.74	−0.55	0.29
HD 175305	−1.40	1.63	0.73	1.30	0.85	−0.13	0.44	−0.45	0.10
HD 186478	−2.58	0.70	−0.35	0.42	−0.22	−1.40	−0.78	−1.50	−0.80
HD 187111	−1.74	...	0.25	1.38	0.49	−0.46	−0.15	−0.87	...
HD 204543	−1.84	1.06	0.28	0.96	0.65	−0.35	0.25	−0.87	0.05
HD 206739	−1.58	1.42	0.66	1.02	0.60	−0.53	0.16	−0.72	0.00
HD 214362	−1.90	...	...	...	0.70	...	...	...	...
HD 216143	−2.18	1.05	−0.11	0.55	−0.02	−0.90	−0.38	−1.24	−0.45
HD 218857	−1.86	1.05	0.21	0.74	0.30	−1.00	−0.42	−1.58	−0.60
HD 220838	−1.65	...	0.56	1.05	0.59	−0.63	0.26	−0.84	−0.05
HD 221170	−2.15	...	−0.05	0.80	0.48	−0.43	0.10	−0.84	−0.20
HD 232078	−1.54	...	0.60	1.40	0.65	−0.20	0.65	−0.63	...
CD −24°1782.....	−2.70	0.10	−0.22	0.40	−0.95	−1.15	−0.60	< −1.70	< −1.25
CD −23°72	−1.17	...	...	...	1.30	...	...	...	...
BD −18°5550.....	−2.93	...	...	...	−1.70	...	...	−2.49	...
BD −15°5781.....	−2.36	...	...	...	−0.80	...	...	...	...
BD −11°145	−2.28	...	...	...	0.10	...	...	...	...
BD −3°5215	−1.16	...	...	...	1.43	...	...	−0.09	...
BD −1°2582	−2.25	...	...	...	1.38	...	...	...	...
BD +1°2916	−1.99	...	0.18	1.25	0.21	−0.42	−0.07	−0.83	...
BD +3°2782	−2.03	...	...	...	0.13	...	...	...	...
BD +4°2466	−2.00	...	...	...	1.73	...	...	...	...
BD +6°648	−2.10	1.15	0.11	0.83	0.18	−0.75	−0.26	−1.30	−0.60
BD +9°2870	−2.37	0.33	−0.38	0.28	−0.70	−1.68	−1.27	−2.11	−1.50
BD +9°3223	−2.26	0.80	−0.02	0.78	0.28	−0.84	−0.59	−1.33	−0.81
BD +11°2998.....	−1.17	1.53	0.84	1.60	1.10	−0.12	0.23	−0.60	−0.12
BD +17°3248.....	−2.02	1.43	0.28	1.08	1.08	−0.20	0.36	−0.55	0.04
BD +18°2757.....	−2.19	...	...	...	0.29	...	...	...	...
BD +18°2890.....	−1.58	...	...	...	0.81	...	...	...	...
BD +30°2611.....	−1.49	...	0.55	1.15	0.72	−0.12	0.78	−0.53	...
BD +52°1601.....	−1.58	...	...	...	0.70	...	...	...	...
BD +54°1323.....	−1.65	1.82	0.45	1.15	0.85	−0.32	0.14	−0.67	0.10
BD +58°1218.....	−2.72	0.35	−0.58	−0.06	−1.09	−1.80	−1.19	−2.00	−1.25

that from the λ6141 line. The λ4554 line is much stronger and more sensitive to microturbulence than the λ6141 line. Microturbulence was not well determined in the PSK study because that study made use of only weak lines. The Ba abundance disparities were eliminated by raising the microturbulence slightly ($\leq$0.2 km s^{-1}) from the PSK value in the few stars where the two lines disagreed.

The Sr II lines used in our analysis are also sensitive to microturbulence. Increasing the microturbulence to bring the two Ba II lines into agreement also decreased the Sr abundance in these same stars by $\simeq$0.15 dex. Because the Sr II lines become so strong in stars cooler than 4500 K, we were unable to derive reliable Sr abundances in such stars. Sr abundances in warmer stars appear to be more reliable.

Tables 3 and 4 present our final *n*-capture element abundances. Table 3 gives the metal-to-iron ratios [m/Fe] and Table 4 gives the absolute log ϵ abundances. The total sample of stars included in Tables 1 and 3 is 70; Eu equivalent widths from Gilroy et al. (1988) were used to redetermine abundances for eight stars (noted in Table 1) for which new blue spectra were not available.

Many of the Bond giants have been studied by previous authors, allowing us to compare our results with the literature. For the six stars in common with Gilroy et al. (1988), our analysis results are in agreement, with a scatter of about 0.20 dex. Our study also includes four stars in common with Gratton & Sneden (1994), and for most elements our log ϵ values are higher by about 0.17 dex.

For the five stars in common with the study by McWilliam et al. (1995a) and McWilliam (1998), we find a mean difference in [Ba/H] of +0.21 dex, in the sense this paper *minus* McWilliam. This difference does not result from the measured line strengths, since the equivalent widths show generally good agreement. Hyperfine/isotopic line structure assumptions cannot be the cause of the discrepancy, as they are the same in here and in McWilliam (1998). Examination of the McWilliam et al. (1995a) model atmosphere parameters compared to ours for the stars in common suggest that the primary sources of the discrepancy in the Ba abundances are differences in the adopted microturbulences. Our microturbulence values are, on average, lower by 0.75 km s^{-1}. Adopting the McWilliam et al. microturbulences with our models brings the abundances into good agreement. Since our spectra are typically of higher signal-to-noise ratio than those available to McWilliam et al., and our microturbulence values are supported by consistency of the Fe II, Ti II, and Ba II abundances from different lines, as described above, we retain our original microturbulence values. For other elements (which are less sensitive to microturbulence), we agree on average to within $\pm$0.2 dex, although the number of stars in common for these other elements is often only two or three. There appears to be no systematic difference between our abundances and those of McWilliam et al. Overall, our abundances appear to be in good agreement with other published values.

4. *N*-CAPTURE ELEMENT ABUNDANCES

4.1. *Star-to-Star Variations*

We first consider whether the star-to-star scatter in the [*n*-capture element/Fe] abundance ratios seen by Gilroy et al. (1988) and by McWilliam (1998) from poorer quality spectra is also present in our data. Figure 3 compares the spectra of BD +9°2870 and HD 6268, two stars

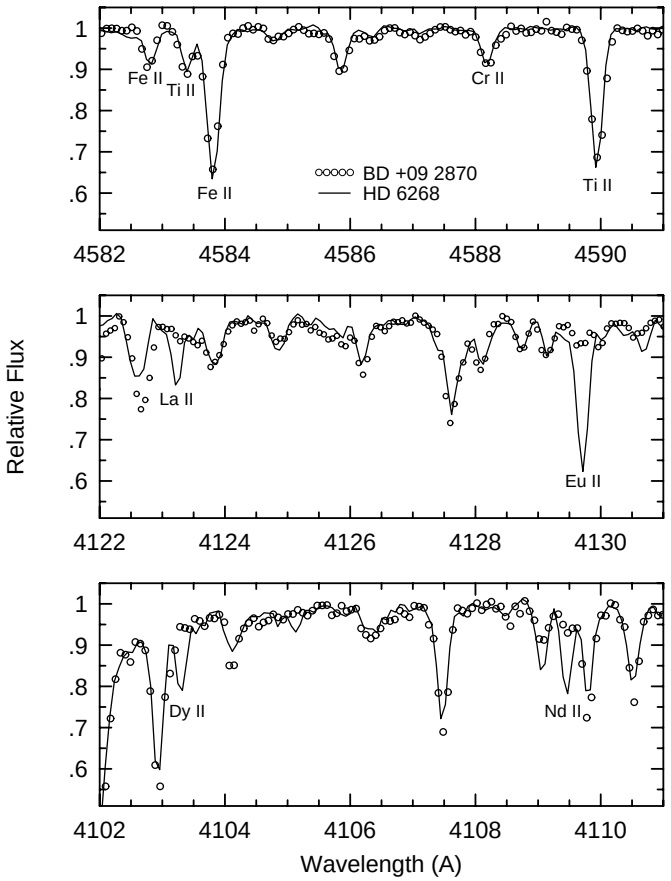

FIG. 3.—Spectral comparison at three wavelengths between two metal-poor stars with similar metallicities and atmospheric parameters, BD +9°2870 (*open circles*) and HD 6268 (*solid line*). Note the similarity of Fe-peak lines in the upper panel and the difference in strength in the *n*-capture lines in the lower two panels.

with similar atmospheric parameters and metallicity ($T_{\rm eff}$/log g/v_t/[Fe/H] = 4650/1.50/1.65/–2.4). The spectral region displayed in the top panel shows that the Fe II, Cr II, and Ti II lines have nearly identical strengths in the two stars. The second and third panels display regions containing *n*-capture lines. Despite the close match of the Fe-peak lines, ionized transitions of the *n*-capture elements Eu, La, Dy, and Nd are 4–10 times stronger in HD 6268 than in BD +9°2870. All of the *n*-capture elements shown here vary together: the strengths of features of La, Eu, Dy, and Nd are always greater in HD 6268 than in BD +9°2870. The *n*-capture element abundances must be different in these two stars.

Star-to-star differences in the *n*-capture element abundances are illustrated in Figure 4, in which we plot the ratios [Eu/Fe], [Dy/Fe], and [Dy/Eu] versus metallicity for the Bond giants. Eu and Dy are both produced primarily by the *r*-process in the solar system (see Appendix and Table 5). For HD 6268 and BD +9°2870 (these stars, whose spectra are shown in Fig. 3, are plotted with special symbols in Fig. 4) the derived Eu and Dy abundances are, as expected, much greater in the star with stronger *n*-capture lines. The ratio of [Dy/Eu] (*bottom panel*), however, is the same in these two stars. The abundances of Dy and Eu vary together in all of the stars included in our analysis, and the [Dy/Eu] ratio does not correlate with the iron abundance. The individual [Eu/Fe] and [Dy/Fe] abun-

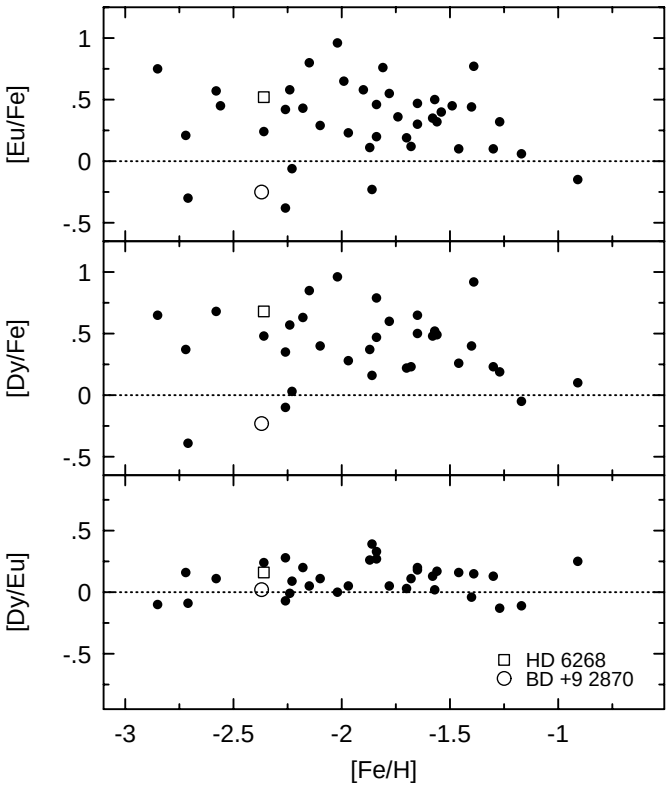

FIG. 4.—Abundance comparisons of (*top panel*) [Eu/Fe], (*middle panel*) [Dy/Fe], and (*bottom panel*) [Dy/Eu] in metal-poor stars. HD 6268 is indicated by an open square and BD +9°2870 by an open circle. The reduction in scatter in the lowest panel compared to the upper panels reflects the strong correlation between the measured Eu and Dy abundances and establishes that the scatter is not the result of observational uncertainty.

dances vary by up to an order of magnitude from solar, but this large scatter is not seen in [Dy/Eu], as it would if caused by observational error. The [Dy/Eu] ratios cluster tightly around the solar ratio for the whole metallicity range studied. These results, particularly the correlation between the Dy and Eu abundances, indicate that the scatter of the *n*-capture elements' abundances with respect to iron is real in metal-poor halo stars and is not the result of observational error.

The behavior of all the heavy elements in our study with metallicity is shown in Figure 5. In addition to our data, indicated by filled circles, we have included data from McWilliam et al. (1995a, 1995b) and McWilliam (1998), Jehin et al. (1999), and Edvardsson et al. (1993) and Woolf et al. (1995). These particular studies were selected because they each include at least 20 stars, they include hyperfine splitting in the calculation of synthetic spectra for Ba and Eu, and together they cover the range of metallicity from $-3.5 \leq [\mathrm{Fe/H}] \leq +0.5$. These studies were selected to provide a sample of stars covering this wide metallicity range while minimizing observational scatter and systematic error. The McWilliam et al (1995a, 1995b) sample contains two known or suspected CH stars with *s*-process enrichments, which we have eliminated from further consideration. These stars show characteristically high abundances of traditional *s*-process elements, particularly Ba, compared to other stars of similar metallicity. We have retained the *r*-process–rich star CS 22892−052.

TABLE 5

r- AND *s*-PROCESS SOLAR SYSTEM ABUNDANCES

Element (1)	Z (2)	N_r^b (3)	N_s^b (4)	N_{total}^b (5)	$F_\odot[r]$ (6)	$F_\odot[s]$ (7)
Zn	30	452	231	683	0.66	0.34
Ga	31	16.3	21.5	37.8	0.43	0.57
Ge	32	56.2	52.5	109	0.52	0.48
As	33	5.33	1.46	6.79	0.78	0.22
Se	34	40.3	21.2	61.4	0.66	0.34
Br	35	4.64	0.93	5.57	0.83	0.17
Kr	36	22.7	29.3	52.0	0.44	0.56
Rb	37	2.89	2.90	5.79	0.50	0.50
Sr	38	2.55	20.5	23.1	0.11	0.89
Y	39	1.31	3.34	4.65	0.28	0.72
Zr	40	2.04	8.66	10.7	0.19	0.81
Nb	41	0.11	0.23	0.34	0.32	0.68
Mo	42	0.64	1.33	1.97	0.32	0.68
Ru	44	0.94	0.60	1.54	0.61	0.39
Rh	45	0.29	0.055	0.34	0.84	0.16
Pd	46	0.77	0.62	1.39	0.56	0.44
Ag	47	0.44	0.12	0.55	0.79	0.21
Cd	48	0.77	0.76	1.53	0.50	0.50
In	49	0.12	0.057	0.18	0.68	0.32
Sn	50	1.41	2.18	3.60	0.39	0.61
Sb	51	0.24	0.047	0.29	0.72	0.28
Te	52	3.95	0.98	4.92	0.80	0.20
I	53	0.85	0.05	0.9	0.94	0.06
Xe	54	3.82	0.98	4.79	0.80	0.20
Cs	55	0.32	0.056	0.37	0.85	0.15
Ba	56	0.81	4.66	5.47	0.15	0.85
La	57	0.11	0.34	0.45	0.25	0.75
Ce	58	0.20	0.89	1.10	0.19	0.81
Pr	59	0.082	0.078	0.16	0.51	0.49
Nd	60	0.42	0.38	0.80	0.53	0.47
Sm	62	0.17	0.090	0.26	0.66	0.34
Eu	63	0.091	0.0025	0.093	0.97	0.03
Gd	64	0.28	0.061	0.33	0.82	0.18
Tb	65	0.060	0.004	0.064	0.94	0.06
Dy	66	0.36	0.050	0.41	0.88	0.12
Ho	67	0.081	0.006	0.089	0.93	0.07
Er	68	0.21	0.041	0.25	0.84	0.16
Tm	69	0.031	0.006	0.037	0.84	0.16
Yb	70	0.16	0.076	0.24	0.68	0.32
Lu	71	0.031	0.008	0.039	0.79	0.21
Hf	72	0.080	0.076	0.16	0.51	0.49
Ta	73	0.013	0.009	0.022	0.60	0.40
W	74	0.062	0.074	0.14	0.46	0.54
Re	75	0.047	0.0045	0.052	0.91	0.09
Os	76	0.65	0.059	0.71	0.92	0.08
Ir	77	0.65	0.005	0.66	0.99	0.01
Pt	78	1.30	0.07	1.37	0.95	0.05
Au	79	0.18	0.010	0.19	0.95	0.05
Hg	80	0.15	0.20	0.35	0.42	0.58
Tl	81	0.053	0.10	0.15	0.34	0.66
Pb	82	0.62	2.3	2.94	0.21	0.79
Bi	83	0.093	0.051	0.14	0.65	0.35
Th	90	0.042	0.0	0.042	1.00	0.00
U	92	0.024	0.0	0.024	1.00	0.00

Our abundances confirm the trend of increasing scatter in the [*n*-capture/Fe] element ratios with decreasing metallicity noted previously by Gilroy et al. (1988) and McWilliam (1998). As metallicity increases, the scatter in the [*n*-capture element/Fe] ratios declines dramatically. At low metallicity, the scatter is astrophysical in origin and not the result of observational uncertainty. At higher metallicities the scatter essentially disappears. We agree with earlier

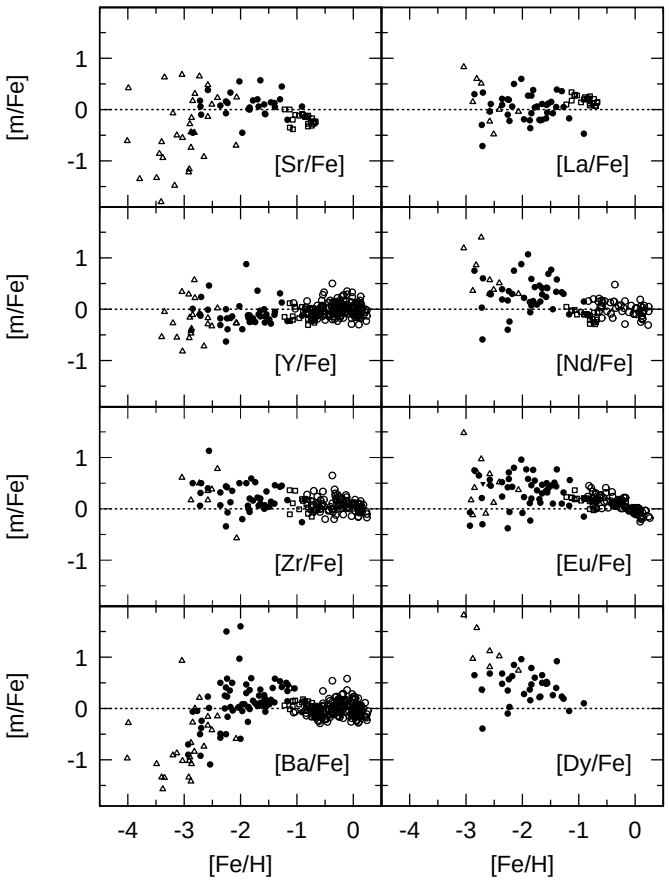

FIG. 5.—[Sr/Fe], [Y/Fe], [Zr/Fe], [Ba/Fe], [La/Fe], [Nd/Fe], [Eu/Fe] and [Dy/Fe] as a function of metallicity. Filled circles are from this paper (filled triangles represent upper limits for Eu and Dy); open triangles are from McWilliam et al. (1995a, 1995b) and McWilliam (1998); open squares are from Jehin et al. (1999); and open circles are from Edvardsson et al. (1993) and Woolf et al. (1995). Note that the McWilliam et al. sample contains two known or suspected CH stars, which have *s*-process element enrichments due to mass transfer from a more massive and evolved companion; these stars have been eliminated from the sample.

studies that such star-to-star variation is most easily explained as resulting from local nucleosynthetic events. Interstellar matter undergoing star formation closer to a site for *r*-process nucleosynthesis, presumably a supernova, might be enriched while other interstellar matter might not. We stress again that the observed star-to-star scatter appears in the total abundance level with respect to iron and not in the relative *n*-capture abundances. The relative abundances are similar in all the extremely metal-poor halo stars, and similar to the solar system *r*-process–only proportions (see Table 5).

4.2. *Abundance Trends with Metallicity*

In this section we examine more closely the abundances of individual *n*-capture elements as a function of metallicity. We look first at the behavior of [Ba/Fe], since Ba abundances are available for stars of lower metallicity than most other *n*-capture elements because of its relatively higher abundance and its strong lines. The fall in the [Ba/Fe] ratio at very low metallicity ([Fe/H] < -2.5), which has been noted in other studies and is also seen in our data, is thought to result from the changing nature of the nucleosynthesis sources for Ba. In the solar system, Ba is overwhelmingly produced in the main *s*-process (see Table 5 and Appendix) in low-mass (1–3 $M_{\odot}$) stars with a small ($\sim$15%) component from the *r*-process. The initial production of Ba at the lowest metallicities, however, is most likely by the *r*-process alone (Truran 1981), occurring in supernovae resulting from more massive and hence more rapidly evolving stars.

The [Ba/Fe] panel of Figure 5 shows that the transition between a pure *r*-process production of Ba and production dominated by the main *s*-process occurs gradually in the metallicity regime from $-2.75 \leq$ [Fe/H] ≤ -2.2. The Ba abundance already approaches a solar [Ba/Fe] ratio in some stars with metallicities as low as [Fe/H] $= -2.75$, hinting at the presence of some *s*-process material in some stars even at this low metallicity. A metallicity of [Fe/H] $= -2.75$ for the first appearance of material of *s*-process origin is significantly lower than previously indicated. Based on the [Ba/Fe] data alone, however, we cannot discriminate between the appearance of *s*-process material and a scatter in the [*r*-process/Fe] ratio.

For most of the *n*-capture elements, the [*n*-capture/Fe] ratios rise above the solar value (Fig. 5, *dotted line*) before falling back to a solar ratio at a metallicity near [Fe/H] $= -1.0$. These high [*n*-capture/Fe] ratios are a reflection of the time delay for the production of the bulk of the iron in the Galaxy. While high mass Type II supernovae are responsible for some of the iron nucleosynthesis (particularly at very low metallicities), Type Ia supernovae (with longer evolutionary timescales due to lower mass progenitors) are presumably responsible for the majority of Galactic iron production (e.g., Matteucci & Greggio 1986). The observed [*n*-capture/Fe] ratios for more metal-rich stars (i.e., [Fe/H] $\simeq -1.0$) tend downward because of the continued increase in Galactic iron production. We caution that disk stars may behave in a different manner than halo stars, and comparisons between these populations could be dangerous. However, the downward trend as a function of increasing metallicity is evident for all of the *n*-capture elements observed except Y, including the *r*-process elements Eu and Dy and the *s*-process element Ba, in all of the halo and disk stars where data are available. The disk and halo populations overlap in metallicity near [Fe/H] $\simeq -1$, and the mix of populations does not appear to cause an increase in the scatter of the [*n*-capture element/Fe] ratios. The onset of the bulk iron production must have occurred at a higher metallicity and presumably at a later time than the onset of Galactic main *s*-process production.

Sr is also produced primarily by the *s*-process in the Solar System. Like [Ba/Fe], [Sr/Fe] is low in very metal poor stars, rising above a metallicity [Fe/H] $= -3.0$ to extend above the solar [Sr/Fe] ratio, and then turning over in the abundance ratio with the increasing formation of Galactic iron. The scatter also decreases at higher metallicities as it does for [Ba/Fe]. However, the scatter appears to be larger in the [Sr/Fe] data, particularly at very low metallicity, than in the [Ba/Fe] data, as noted previously by Ryan et al. (1996). This might reflect the influence of an additional or different production mechanism for Sr at very low metallicity (see discussion in § 4.4) or perhaps somewhat less certain observational data for this element at the lowest metallicities.

The abundance trends for the other elements shown in Figure 5 are in general the same as shown for Ba and Sr, but with much less complete data sets. Thus, for example,

[Y/Fe] and [Zr/Fe] do not show the rapid increase in abundance at low metallicities, but there are, in fact, not much data for those elements at the lowest metallicities. We have already seen that Eu and Dy are correlated at the lowest metallicities, although there is much less data available for Dy at higher metallicities. (Dy was not included by Edvardsson et al. 1993 or Woolf et al. 1995, or by Jehin et al. 1999.) The turnover in [m/Fe] at increasing iron abundance and the increased scatter at lower metallicities is exhibited by all of the elements shown in Figure 5 (except Y). Although the abundance data for Eu and Dy are limited or nonexistent at [Fe/H] $\simeq -3.0$, these elements do not seem to share the characteristic of a decline in abundance relative to iron at [Fe/H] < -2.4 seen in the traditional *s*-process elements Ba and Sr. Indeed, as we will see later, the average abundance of these elements at [Fe/H] $= -2.8$ is still well above solar, even when the *r*-process rich star CS 22892−052 is excluded from the average.

4.3. *Heavier N-Capture Elements* Ba–Dy

The *r*-process element Eu has frequently been contrasted with Ba, made predominantly in the *s*-process in solar material (see Table 5 in Appendix and Figure 11). The ratio of these two elements is often used to identify *n*-capture nucleosynthesis mechanisms. The logarithmic abundances of the two elements are plotted in Figure 6, following Woolf et al. (1995). In addition to our giants, we have included the same literature data sets as in Figure 5. Superimposed on the data are a dotted line for the scaled solar system *r*-process–only abundance ratio and a solid line for the scaled total solar system abundance ratio. For the lowest metallicities [i.e., log ϵ(Ba) < 0.0], the [Ba/Eu] ratio is constant and equal to the scaled solar system *r*-process–only abundance ratio.

Eu is made only by the *r*-process and Figure 6 clearly indicates that at low metallicities (certainly at or below [Fe/H] = –2.75), Ba is made in the same way. This suggestion has been made previously (Spite & Spite 1978; Truran 1981) based upon data for a few individual, metal-poor stars. Sneden et al. (1996, 1998) and Cowan et al. (1999) showed that the well-studied ultra–metal-poor star CS 22892−052 ([Fe/H] $= -3.1$), for example, has a *n*-capture signature that is totally consistent with *r*-process–only *n*-capture nucleosynthesis. Here we observe the same (solar *r*–process only) ratio of Ba/Eu in many stars at low metallicity, suggesting that Ba and Eu are systematically made together in the *r*-process during the early history of the Galaxy. Other suggestions (e.g., an early Galactic *s*-process origin) for the Ba/Eu ratio in these stars seem unlikely. (See also McWilliam 1998.) The site(s) that produced Ba and Eu in the solar system *r*-process–only ratio in these very metal-poor halo stars must have evolved rapidly during the early history of the Galaxy to synthesize the *n*-capture elements while the Fe abundance was still very low (see also Raiteri et al. 1999).

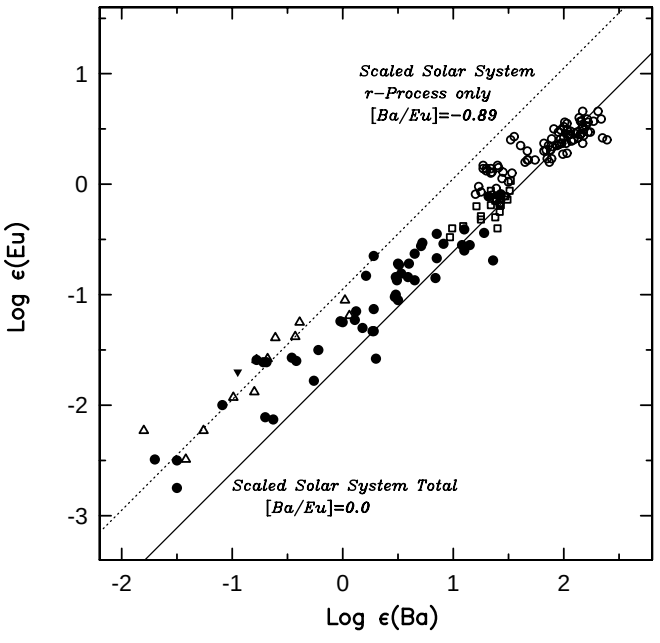

FIG. 6.—Log ϵ(Eu) vs. log ϵ(Ba). The dotted line indicates the solar system *r*-process abundance ratio and the solid line indicates the total solar system abundance ratio of Ba/Eu. The symbols are as in Fig. 5.

Referring again to Figure 6, we note that the Ba/Eu abundance ratio changes near log ϵ(Ba) = 0 from the characteristic *r*-process value to the value found for the total solar system mixture of *r*-process plus *s*-process contributions. As the data in Table 3 indicate, this corresponds to a stellar metallicity range from $-2.4 <$ [Fe/H] < -2.1. At this metallicity, the ratio of Ba/Eu increases as a result of increased production of Ba, but not Eu. For stars with [Fe/H] above this metallicity, the [Ba/Eu] ratio seems to reflect substantial production of Ba by the *s*-process. This transition marks the main onset of Galactic *s*-processing at this metallicity, sometime after the earlier onset of *r*-process synthesis. This delay in *s*-processing is consistent with a longer stellar evolutionary timescale typical of low-mass (1–3 $M_\odot$) stars, thought to be the site for this type of *n*-capture synthesis (Gallino et al. 1998). The gradual rise in the Ba/Eu ratio suggests that the *s*-processing sites must include a range of stellar masses. Some *s*-process material may already be present at [Fe/H] $= -2.75$ in a few stars, but the bulk of the *s*-processing is delayed until near [Fe/H] $= -2.2$. The change in the Ba/Eu ratio near [Fe/H] $= -2.2$ is probably caused by the (main) *s*-process occurring in the most massive (perhaps 2–3 $M_\odot$) of these low-mass stars, with additional *s*-process contributions coming from increasingly lower mass stars as the Galaxy ages. The gradual rise in the [Ba/Eu] ratio over several tenths of a dex in [Fe/H] is inconsistent with s-process production being limited only to stars of $\sim 1\ M_\odot$, which take 10^{10} years to evolve to the AGB stage, and may indicate local mixing effects and a range of stellar mass progenitors for the main *s*-process production. Somewhat more massive AGB progenitors (2–3 $M_\odot$) may deposit their ejecta earlier than the more uniformly distributed and more numerous low-mass (1–2 $M_\odot$) AGB stars.

The Ba and Eu abundances in Table 4 can also be used to estimate the fraction of Ba produced by the *r*- and *s*-process in each star, using the assumptions that Eu is produced only by the *r*-process and that the *r*-process ratio of Ba/Eu is given by the *r*-process–only fractional abundances in the Sun. Between 50%–80% of the Ba in most stars in our halo sample with [Fe/H] ≥ -2.0 is produced by the *s*-process. Detailed analyses of the abundances of the metal-poor star HD 126238, with [Fe/H] $= -1.7$ (Cowan et al. 1996), found that only a small percentage (20%) of the Ba could be attributed to the *s*-process in that star. Our sample includes three other stars with metallicities near [Fe/H] $= -2.0$ that

have relatively low *s*-process fractions (i.e., <40%). Cowan et al. (1996) suggested that at a metallicity of [Fe/H] = −1.7, the *s*-process fraction was coming only from the most massive AGB sites. Only at higher metallicities ([Fe/H] > −1.5) do most of the stars have Ba *s*-process fractions at or near the solar value of 80%. The relative paucity of AGB stars with masses near $\simeq 3\ M_\odot$ might well account for some of the dispersion in the [Ba/Fe] ratio in stars at intermediate metallicity (−2.0 < [Fe/H] < −1.0). More metal-rich stars, formed after a time when more numerous and more ubiquitous lower mass ($\simeq$1.5–3 $M_\odot$) AGB stars are contributing *s*-process elements, are increasingly uniform in their [Ba/Fe] ratio. The major (low-mass, perhaps 1–1.5 $M_\odot$) sites have not evolved to produce *s*-process elements until such time as the Galactic iron abundance has reached [Fe/H] ∼ −1.0. At this metallicity, the Galaxy contains a mixture of different stellar populations, which may well confuse the interpretation of Galactic chemical enrichment history.

The appearance of major phases of production of heavy elements in the Galaxy can be seen by considering the abundances of *r*- and *s*-process element fractions separately. In Figure 7 we plot the *r*-process–only and *s*-process–only abundances of barium as a function of [Fe/H], following Raiteri et al. (1999). Note that the "solar" ratios in Figure 7 are not the total [Ba/Fe] ratio, but the portions of Ba attributed to just the *r*- or *s*-process. The *r*-process–only [Ba/Fe] ratio is just equal to the [Eu/Fe] ratio, since Eu is produced almost entirely (97%) by the *r*-process, and the Ba/Eu *r*-process ratio is fixed at the *r*-process–only ratio. For stars more metal-poor than [Fe/H] < −2.75, for which there is no main *s*-process contribution, the total Ba abundance can be used directly. The *s*-process–only barium abundance is simply what is left after the *r*-process Ba is subtracted from the total observed abundance. In those cases where the computed number of *r*-process–only barium atoms exceeds the total number of barium atoms observed, we have set the *r*-process–only barium abundance to the total observed value and the *s*-process–only value to zero [i.e., $\log \epsilon(\mathrm{Ba}_{s\text{-process}}) \ll 0$].

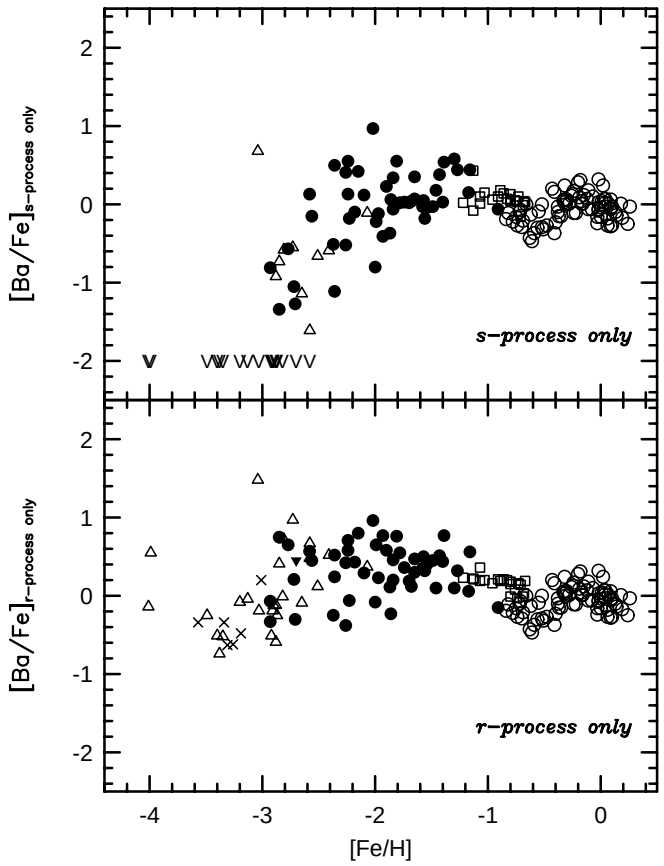

FIG. 7.—[Ba/Fe] vs. [Fe/H] for the *r*-process–only (*lower panel*) and *s*-process–only portions of Ba. The *r*-process and *s*-process fractions were computed as described in the text. The symbols are as in Fig. 5, with the addition of crosses for stars from Ryan et al. (1996). The downwardly directed arrows in the upper panel mark the position of stars which do not appear to contain *s*-process material.

In the upper panel of Figure 7, *s*-process Ba first appears at a metallicity [Fe/H] = −2.75, with the bulk of *s*-process production delayed until [Fe/H] ∼ −2.4, consistent with the shift in the Ba/Eu ratio seen in Figure 6. The downwardly directed arrows in the upper panel of Figure 7 mark the metallicities of stars that do not appear to contain *s*-process material. The existence of a wide (in metallicity) transition region during which the Galactic *s*-processing gradually appears may also explain why there might have been a "controversy" in the past, with some authors suggesting on the basis of a single star that there was significant *s*-process, rather than only *r*-process production early (i.e., at low metallicity) in the Galaxy.

While the heavy elements ($Z \geq 56$) at low metallicity are produced only by the *r*-process, the rise in $[\mathrm{Ba}_{r\text{-process}}/\mathrm{Fe}]$ indicates a significant increase in production of *r*-process elements near a metallicity [Fe/H] = −2.9. The delay in the production until this metallicity may be related to an evolutionary timescale for the stellar source of the *r*-process, suggesting that most *r*-process elements are produced in relatively low-mass (e.g., 8–10 $M_\odot$) Type II supernovae (Mathews & Cowan 1990; Wheeler, Cowan, & Hillebrandt 1998; Ishimaru & Wanajo 1999; Travaglio et al. 1999). Such stars do not evolve quickly enough to contribute *r*-process elements at earlier time (presumably even at the lowest metallicities), producing a discontinuity when they do begin to contribute. The transition in $[\mathrm{Ba/Fe}]_{r\text{-process}}$ at [Fe/H] = −2.9 is qualitatively different than the gradual *s*-process–only transition at [Fe/H] = −2.4. Despite some dispersion, *r*-process element abundances (with respect to metallicity) rise relatively sharply, indicating a somewhat narrow range of stellar masses for *r*-process production. These *r*-process abundances in extremely metal-poor stars are consistent with the other studies listed above that suggest low-mass supernovae as the site for the production of the heavier *r*-process elements. Our data alone, however, are insufficient to determine the precise mass range (e.g., whether 8–10 $M_\odot$ stars are responsible) for such sites of *r*-process production.

The presence of Ba in stars more metal-poor than [Fe/H] = −3.0 suggests either contributions from an additional, earlier (i.e., more massive than 8–10 $M_\odot$) source for the heavier *r*-process elements or perhaps a range of *r*-process/Fe yields in more massive SN IIs. We note, however, that other studies suggest that such a range of yields must be relatively small, and likewise any alternative *r*-process sources must have conditions somewhat similar to those found in the standard *r*-process for the production of the heavier *n*-capture elements. This follows since the abundances of the heavier *n*-capture elements in ultra–metal-poor stars, such as CS 22892−052 ([Fe/H] = −3.1), show

a scaled solar system *r*-process pattern. This close adherence to the solar system *r*-process pattern implies a relatively narrow range of either nuclear or astrophysical conditions and thus constrains any alternative *r*-process production or range of *r*-process/Fe yields to explain the *n*-capture abundances in the early Galaxy. Thus, for example, the Ba may be produced by a few rare, more massive Type II supernovae or perhaps by some other process that operates in stars with masses greater than 10 solar masses. Note that these more massive supernovae, which may contribute only modest amounts of *r*-process elements, do produce Fe.

Ryan et al. (1996) provide Ba abundances for a few stars as metal-poor as [Fe/H] = −3.6, which are in agreement with similar metallicity stars in the McWilliam et al. sample. These stars are plotted in Figure 7 as crosses to demonstrate one additional point: that the large scatter seen in the $[Ba/Fe]_{r\text{-process}}$ abundances at metallicities [Fe/H] > −2.75 is gone at lower metallicity. While Ba abundances are available for only a few stars (eliminating CH/CN-strong stars that may be contaminated from a companion), the rms scatter of stars from −3.6 < [Fe/H] < −3.3 is comparable to the scatter observed in stars near solar metallicity. To the extent that this reduction in scatter is not the result of observing Ba only in stars that are *n*-capture–rich, the low scatter prior to the onset of the bulk of the *r*-process production at [Fe/H] = −2.9 may constrain the process producing *n*-capture elements at ultra–low metallicity.

Two stars at [Fe/H] = −4.0 in the lower panel of Figure 7 deserve also further comment. These stars, CD −38°245 and CS 22949−037, have apparent Ba abundances higher by 0.5 dex than similar giants at [Fe/H] = −3.5. (We note that a spectrum from J. E. Norris (1999, private communication) confirms the relatively high Ba abundance in CD −38°245.) Do these giants foretell a rise in the [*r*-process/Fe] ratio at still lower metallicity? Additional observations of Ba in other stars at [Fe/H] = −4.0 are needed to determine the behavior of the *r*-process ratio at extremely low metallicity.

4.4. *Lighter N-Capture elements:* Sr, Y, *and* Zr

While the abundances of the heavier ($Z \geq 56$) *n*-capture elements can be understood with the *r*-process early in the history of the Galaxy and with *s*-process contributions (to at least Ba) occurring at higher metallicities and later times, the origin of the lighter *n*-capture elements is not as easily explained. Unfortunately, the only elements below Ba that have so far been accessible are Sr, Y, and Zr. In Figure 8 we illustrate the behavior of Y and Ba with respect to Sr. In the top panel we show log ϵ(Ba) versus log ϵ(Sr). The data sets shown are the same as in Figure 5. Superimposed on the data are the scaled solar system *r*-process abundances (*dotted line*), the scaled total solar system abundances (*solid line*), and an assumed composition of 10% *r*-process and 90% weak *s*-process production (*dashed line*). The weak *s*-process yields have been taken from Raiteri et al. (1993). In Figure 9, which plots [Sr/Ba] versus [Fe/H], we see a very large scatter in the Sr/Ba abundance ratio for the lowest metallicity ([Fe/H] < −2.5) stars. While some of this scatter may be due to observational uncertainties in the Sr abundance, an additional nucleosynthesis source is required to explain the behavior of Sr and the increase in the Sr/Ba ratio at the lowest metallicities.

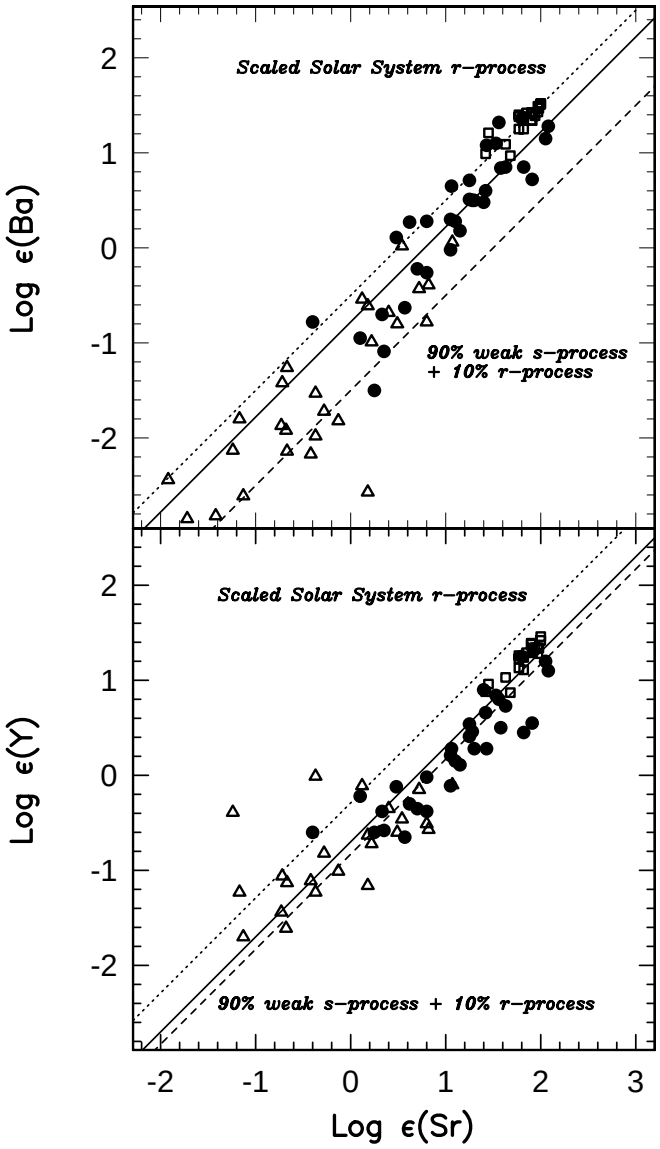

FIG. 8.—Log ϵ(Ba) (*upper panel*) and log ϵ(Y) (*lower panel*) vs. log ϵ(Sr). The dotted lines in both panels mark the solar system *r*-process abundance ratio, the solid lines are the total solar system abundance ratio, and the dashed lines assume a composition of 90% weak *s*-process plus 10% *r*-process. The symbols are as in Fig. 5.

The data for the lowest metallicity stars in Figures 8 and 9 do not fall on the solar system *r*-process–only line. In contrast to the heavier *n*-capture elements, the *r*-process alone cannot account for the observed Sr abundances. In solar system material, a sizable contribution (∼20%) to the Sr abundance (and less for Y and Zr) comes from the weak *s*-process which is expected to occur much earlier in the proto-Galaxy than the main *s*-process component, since it is produced in core He-burning in massive (∼ 25 $M_{\odot}$) stars rather than He-shell flashes in low-mass stars (see Lamb et al. 1977; Raiteri et al. 1993). The enhancement of Sr relative to Ba seems to indicate that there may be an additional *n*-capture contribution to the early synthesis of Sr (in Figs. 8 and 9) with many of the lowest metallicity stars falling on or near the dashed line representing a composition of 10% *r*-process and 90% weak *s*-process (see also Ryan et al. 1996). Not all of the data, however, fall on that line; some, in fact, fall on the *r*-process–only line, suggesting a range of

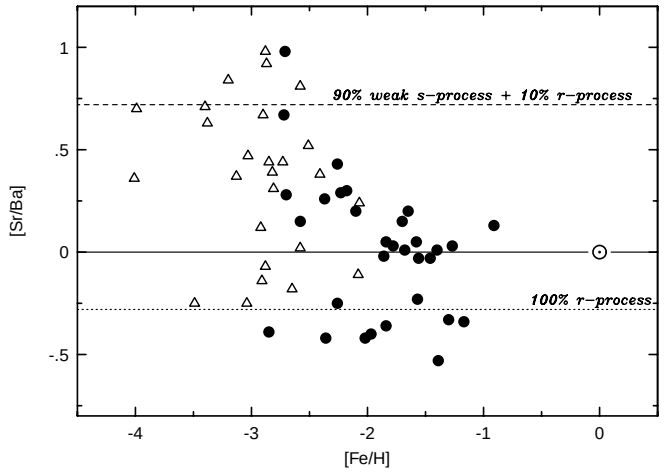

FIG. 9.—[Sr/Ba] vs. [Fe/H] for metal-poor giants. The dashed line indicates a composition of 90% weak *s*-process plus 10% *r*-process, the solid line marks the solar ratio and the dotted line is the solar *r*-process–only ratio. Symbols are as in Fig. 5.

r-process and alternate *n*-capture contributions, in various amounts, may be required to explain the Sr abundances in the lowest metallicity stars. An additional *n*-capture contribution, synthesized in massive stars, to the abundance of Sr at low metallicities may also add to the observed scatter in the Sr/Ba ratios in an inhomogeneously mixed proto-Galaxy, with progenitor stars of perhaps larger masses than those for the *r*-process production. (This assumes low-mass, 8–10 $M_\odot$, Type II SNe progenitors for the *r*-process—see Mathews, Bazan, & Cowan 1992 and Wheeler et al. 1998.) While the weak *s*-process may be responsible for the enhanced Sr, Y, and Zr at [Fe/H] < -3, we caution that at these very low metallicities, contributions from the weak *s*-process may be too small, owing to the low initial iron abundances in the progenitor stars and the secondary nature of this process. (This does not affect *r*-process nucleosynthesis.) On the other hand, the abundances of Sr and Ba are deficient by typically an order of magnitude relative to Fe at this low metallicity.

As in Figure 6, we see a transition region shown by the Sr and Ba data in the upper panel of Figure 8. The shift toward the solar system total line with increasing Sr abundance again indicates an increase in Ba production at later Galactic time. This shift, though broad, occurs near $\log \epsilon(\mathrm{Sr}) = 0.6$–$0.8$, corresponding to [Fe/H] $= -2.2$ to -2.4, similar to the range seen for the Ba and Eu data (see also Fig. 9). Again, this appears to be the onset of the Galactic main *s*-process production affecting the Ba/Sr ratio. (The main *s*-process, coming from $\simeq 1$–$3\ M_\odot$ stars is responsible for all of the *s*-process Ba production—there is no weak *s*-process contribution to Ba synthesis.) Although there is still some scatter, most of the more metal-rich stars fall along the total scaled solar system abundance (*solid*) line, as expected.

The lower panel in Figure 8 shows the behavior of Y, also primarily an *s*-process element, with respect to Sr. In general Y and Sr are better correlated than Ba and Sr. At lowest metallicities there is again some scatter, but much less so than in the Ba versus Sr plot in the top panel. While the Y and Sr abundances adhere more closely to the scaled total solar system abundance ratio, the Ba and Sr abundances in the upper panel establish that the main *s*-process cannot be responsible for Sr and Y production at the lowest metallicities included in Figure 8. The Sr and Y abundances are inconsistent with the *r*-process being the main source of these elements in the lowest metallicity stars. While the weak *s*-process makes a more sizable contribution to Sr, Y also has a weak *s*-process component. A mixture of approximately 80%–90% weak *s*-process and 10%–20% *r*-process material is a good match to the observed Y and Sr abundances in the lowest metallicity stars. Both the weak *s*-process line and the total solar system (*solid*) line are very close together, and at higher metallicities the data appear to follow the total solar system line, consistent with the dominant production being by the main *s*-process for those higher values of [Fe/H]. Observations of the Zr abundance at lower metallicities would be useful to confirm the contributions of any alternate *n*-capture process in the early Galaxy.

Other alternative *n*-capture mechanisms, in addition to the weak *s*-process, have also been suggested to account for the abundances of Sr, Y, and Zr. Based upon solar system meteorite data, a second, separate *r*-process site has been suggested, with one *r*-process site for those elements above Ba and a different site for the lighter *n*-capture elements (Wasserburg, Busso, & Gallino 1996; Qian, Vogel, & Wasserburg 1998). In addition to massive stars (Woosley et al. 1994) and low-mass supernovae (Mathews et al. 1992; Wheeler et al. 1998), neutron-star binaries have also been suggested as possible *r*-process sites (Lattimer et al. 1977; Mathews et al. 1992; Rosswog et al. 1999). Examination of our data, particularly Figures 5–10, does seem to indicate a different origin for the elements Sr-Y-Zr than for the heavier *n*-capture elements. We can speculate that the presence of *r*-process material early in the history of the Galaxy, at very low metallicity, might suggest supernovae as a likely source for the heaviest *n*-capture elements, with (perhaps) binaries contributing at later times and more infrequently to the lighter *n*-capture abundances. We caution at this point that

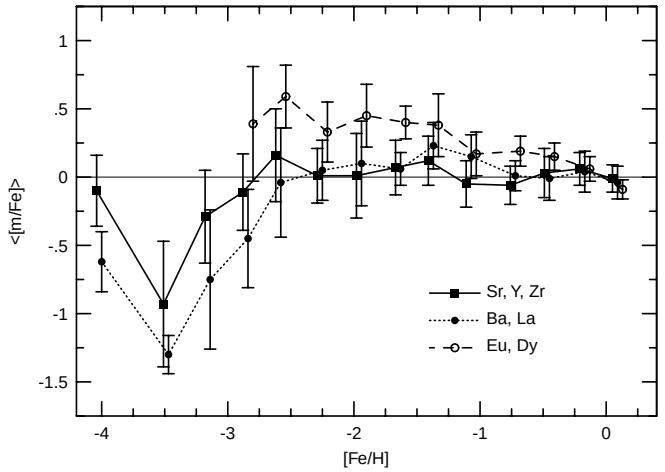

FIG. 10.—$\langle$[m/Fe]$\rangle$ vs. [Fe/H]$\rangle$ and rms scatter vs. [Fe/H] for Sr-Y-Zr (*filled squares* and *dotted line*), Ba-La (*filled circles* and *solid line*) and Eu-Dy (*open circles* and *dashed line*). The data are from this paper, from McWilliam et al. (1995a, 1995b) and McWilliam (1998), Jehin et al. (1999), Ryan et al. (1996), and Edvardsson et al. (1993) and Woolf et al. (1995). Plotted are the geometric means of the abundances and the rms scatter computed in number space. The [Fe/H] values have been shifted slightly to avoid overlaying the error bars. Note the reduction in the scatter of the Ba-La abundances at [Fe/H] $= -3.5$. The bin at [Fe/H] $= -4.0$ contains only two stars.

the stellar data for the lighter *n*-capture elements, and especially the elements between Zr and Ba, are still not extensive enough to lead to an unambiguous explanation for the origin of these elements, and more abundance data and theoretical work will be required.

4.5. *Galactic Chemical Evolution*

We see further evidence of the extent and nature of the scatter in the abundances as a function of metallicity in Figure 10. This figure plots the geometric means ($\langle$[m/Fe]$\rangle$ computed in log space) for the elements Sr-Y-Zr, Ba-La, and Eu-Dy. The stars have been binned in steps of 0.3 dex, except for the lowest metallicity range ([Fe/H] < -3.6) for which there are very few stars. The Eu and Dy abundances for stars more metal-poor than [Fe/H] < -3.0 have been omitted. These elements have been measured in only two such metal poor stars (CS 22892−052 and CS 22952−015), with a few stars showing only upper limits. (A selection bias may favor *r*-process–rich stars.) The rms error bars (computed in number space) are shown for each group of elements. Note that the lowest metallicity bin at [Fe/H] = −4.0 contains only two stars.

Figure 10 illustrates the increase in scatter for *all* of the elements as metallicity decreases to [Fe/H] = −3.0, supporting our earlier contention that at early times (i.e., metallicity) the proto-Galaxy was not chemically well mixed. The data support the suggestion of individual nucleosynthetic effects (e.g., supernovae) affecting different regions of the proto-Galaxy with different total amounts of synthesized material. At even lower metallicity, the scatter in Sr-Y-Zr (mainly Sr at this low metallicity) continues to increase, while the scatter in Ba-La (mainly Ba) seems to decrease, as mentioned earlier in § 4.3.

Figure 10 also demonstrates that the overall scatter seems to have dropped to zero, and the mean abundances are roughly consistent with solar values, by the time [Fe/H] = −0.6. This presumably marks the metallicity (and some associated Galactic time) when the stellar chemical abundances have become homogenized and when the Galaxy became more thoroughly chemically mixed (see also McWilliam 1998). This may also be related to the disk-halo transition.

At very low metallicities ([Fe/H] ≤ -2.5), the average abundance relative to Fe of the elements Sr, Y, Zr, Ba, and La is significantly subsolar, indicating that the production of many *n*-capture elements lags behind early Galactic iron production (presumably from stars above 10 $M_{\odot}$). As metallicity increases above [Fe/H] ~ -2.0, the average abundances of these heavy elements relative to Fe may rise slightly above solar values. For the heavier *r*-process elements Eu and Dy, the abundances are markedly supersolar, and they show no evidence for the decline characteristic of the "*s*-process" elements at [Fe/H] < -2.5. Later, presumably with the increasing iron production from Type I supernovae, beginning at [Fe/H] ~ -1.5, the abundance ratios tend downward toward solar values, suggesting that iron production is not tied to the same astrophysical site as *r*-process nucleosynthesis. Instead, it may be that supernovae from only a narrow mass range of perhaps 8–10 $M_{\odot}$ (i.e., low-mass) stars are responsible for *r*-process nucleosynthesis (Mathews & Cowan 1990; Wheeler et al. 1998; Ishimaru & Wanajo 1999; Travaglio et al. 1999), while early iron synthesis is coming from a different range of massive stars producing Type II supernovae. Furthermore, if the neutron-capture elements and iron are both coming from Type II supernovae, our data implies that the [*r*-process/Fe] ratio of the ejecta must exceed the solar ratio and that the *r*-process abundance is increasing at a faster rate than the Fe abundance early during the epoch after the first 8–10 $M_{\odot}$ stars become supernovae and before the Type Ia supernovae begin to contribute Fe. Alternatively, other possible *r*-process sites might also participate in this early Galactic *r*-process nucleosynthesis, and would not be involved in iron synthesis. One such suggested site, for example, is neutron star-binaries (see Mathews et al. 1992; Rosswog et al. 1999). (See also Cowan, Thielemann, & Truran 1991 for a discussion of possible *r*-process sites.)

Figure 10 also demonstrates a difference in the behavior between the lighter (Sr-Y-Zr) and the heavier (Ba-La and Eu-Dy) *n*-capture elements. For example, the abundances of Sr, Y, and Zr are significantly higher than Ba and La at very low metallicities, as expected if an additional production mechanism occurring in massive stars is involved. As we have noted earlier, at metallicities above −2.75, both Sr, Y, and Zr and Ba and La are produced in the main *s*-process, while several of the heavier elements, notably Eu and Dy are produced primarily in the *r*-process. The difference in the mean values may reflect the evolution of the different (mass) sites for these synthesis processes. Some contribution to the scatter in the lighter element data at metallicities [Fe/H] < -2 may be from the weak *s*-process coming from massive stars.

4.6. *Abundances at Very Low* ([Fe/H] < -3.5) *Metallicities*

We end this discussion of the abundances by stressing the need for additional data for stars with [Fe/H] < -3 to draw any conclusions on the nature of the early synthesis of these *n*-capture elements. Thus, for example, if Ba and Fe are both produced (early in the Galaxy) in Type II supernovae, can we expect that the [Ba/Fe] abundance ratio should remain constant at [Ba/Fe] = −1.3 at lower metallicity (e.g., $-3.5 <$ [Fe/H] < -4.5)? Should the [Ba/Eu] ratio also remain constant at [Ba/Eu] = −0.89? Observations of [Ba/Fe] and [Eu/Fe] at very low metallicity would also help to confirm whether low-mass (8–10 $M_{\odot}$) Type II supernovae are the dominant site for the *r*-process, and to identify the site of any *r*-process nucleosynthesis at earlier Galactic time. Such observations may be difficult, however, considering the weakness of the Eu II lines in most giants already at [Fe/H] = -3.0, and of even the Ba II lines at [Fe/H] = −4.0. Observations are also needed at very low metallicities for Y and Zr to see if they mimic the trends seen (and presumably the production mechanisms) for Sr. Finally, we note that observations in very low-metal stars of elements between Zr and Ba could help in deciding whether there are, in fact, two separate *r*-process sites and if the production mechanisms in those sites were the same in the early Galaxy as they may be today.

5. CONCLUSIONS

We have presented new *n*-capture abundance results for 43 metal-poor Bond giants and Ba abundances only for an additional 27 metal-poor giants. From these heavy element abundances, we draw five principal conclusions:

1. *The scatter in the abundances of all the n-capture elements from star to star is of astrophysical origin, and the scatter increases as we go to lower metallicities.* Elemental

abundance correlations (e.g., [Dy/Eu] vs. [Fe/H]) demonstrate that all of the observed heavy elements with $Z \geq 56$ vary together, and the observed scatter is not the result of errors in measurement or analysis. Instead, this scatter results from inhomogeneity of the material at early times in the Galaxy's history, presumably because of the mixture of different amounts of supernova nucleosynthesis ejecta products in the gas at different star formation sites. While this result was first noted by Gilroy et al. (1988) and was emphasized by McWilliam et al. (1995b), our new comprehensive data, covering a wider metallicity range, strengthen this contention. As the metallicity increases, and presumably the age of the Galaxy, the scatter decreases, indicating that production from more common sites and/or mixing of the material must be taking place.

2. *The ratio of the abundances of the elements* Ba (*an s-process element in the Sun*) *and* Eu (*an r-process element in the Sun*) *at very low metallicity indicates that the heavy n-capture elements were formed predominantly via the r-process at the earliest times in Galactic history*. The ratio of these elements in the most metal-poor stars is reduced by a factor of 6 compared to the solar composition, and the ratio remains at or near the solar *r*-process value even as the overall abundance of the *n*-capture elements relative to iron varies by more than an order of magnitude. This result, suggested previously based upon a single or a few stars (see Truran 1981; McWilliam et al. 1995b; Sneden et al. 1996, Ryan et al. 1996) is now seen to be characteristic of the halo population in the Galaxy. For these very low-metallicity stars, the relative *n*-capture elemental abundances are consistent with a scaled-solar system *r*-process distribution, at least for elements with $Z \geq 56$. These new results put significant constraints on the types (and specifically the evolutionary timescales) of objects that were the progenitors of the metal-poor halo stars and on the nucleosynthetic conditions that produced the *r*-process elements.

3. *Significant production of r-process elements began when the metallicity of the Galaxy reached* [Fe/H] $= -2.9$. This onset is consistent with the original suggestion by Mathews et al. (1992) that Type II supernovae of a narrow range of initial mass (8–10 $M_{\odot}$) stars are responsible for nucleosynthesis of *r*-process elements. Some *r*-process element production also occurred to produce the *r*-process elements observed at even lower metallicity, perhaps due to rare, more massive Type II supernovae or processes operating in such massive stars. Observations of Ba in stars with metallicities near [Fe/H] $= -4.0$ are needed to understand such early nucleosynthesis.

4. *Our abundance correlations also suggest that an alternate n-capture site is needed for much of the production of the lightest n-capture elements, specifically Sr, early in the history of the Galaxy*. For the most metal-poor stars, the elements Sr, Y, and Zr do not follow the same trends as the heavier *n*-capture elements, indicating that Sr-Y-Zr are probably not formed via the same process as the elements such as Ba, Eu, etc. Sr does correlate with Ba at metallicities above [Fe/H] $= -2.5$ where both elements are produced primarily in the main *s*-process in low-mass AGB stars. For lower metallicities, the Sr/Ba ratio increases and the stars display a large scatter in the Sr/Ba ratio. The lack of a correlation between the Sr and Ba abundances at very low metallicity suggests that different processes are responsible for their formation. For [Fe/H] < -2.8 a combination of the *r*-process and perhaps the weak *s*-process could be responsible for light element *n*-capture production. At [Fe/H] $= -3$ the abundances of Sr and Y are consistent (on average) with a mixture of 80%–90% contributions from the weak *s*-process and 10%–20% contributions from the *r*-process. Note that a correlation of Sr with Ba would not be expected, since the weak *s*-process produces Sr but not Ba or other, heavier, *n*-capture elements. A second *r*-process may also have contributed to the Sr, Y, Zr, and other light ($Z < 56$) *n*-capture element abundances. In order to clarify the processes which produce the light *n*-capture elements in the most metal-poor stars, observations of additional elements lying between Zr and Ba will be needed. Such elements may be produced by the second *r*-process but not the weak *s*-process.

5. *As metallicity increases, s-process contributions from low-mass AGB stars become apparent and finally dominate the* Ba *abundance, leading to the observed solar system ratio of* Ba/Eu. The data indicate the presence of a main *s*-process contribution in some stars as metal-poor as [Fe/H] $= -2.75$, lower than previous studies have suggested, with the major increase in (the bulk of the) Ba production occurring at [Fe/H] $= -2.2 \pm 0.2$. The transition to an *s*-process regime is delineated clearly in our data because of the large sample of stars now available. The transition is difficult to pinpoint without a large sample because of the scatter in [Ba/Fe] at low metallicities and the spread of metallicity over which the transition occurs. The observed decline of Ba relative to Fe at low metallicity is due to the absence of *s*-process contributions to the heavy element abundances below [Fe/H] $= -2.8$, rather than because Ba is a secondary element. The delay in the onset of the *s*-process is consistent with standard models suggesting lower masses (and hence longer evolutionary timescales) for the sites of the *s*-process. However, the onset of the *s*-process in low-mass AGB stars near [Fe/H] $= -2.8$ along with a range of metallicity over which Galactic *s*-processing occurs, suggests both a range of *s*-process progenitors and that the earliest occurrence of Galactic *s*-processing might arise from progenitors more massive than typically assumed for the main *s*-process.

We thank Daryl Willmarth and the staff of the Kitt Peak National Observatory for assistance in obtaining the spectra used in our analysis, and David Arnett, Dave De Young, Inese Ivans, and Craig Wheeler for valuable conversations on the subject of the early chemical enrichment of the Galaxy, and Roberto Gallino for his extensive and thoughtful comments on the manuscript. We also thank referee Andy McWilliam for thoughtful advice that significantly improved this manuscript. Partial support for this research was provided by the National Science Foundation (AST96 18364 to C. S. and AST96 18332 AST99 86874 to J. J. C.).

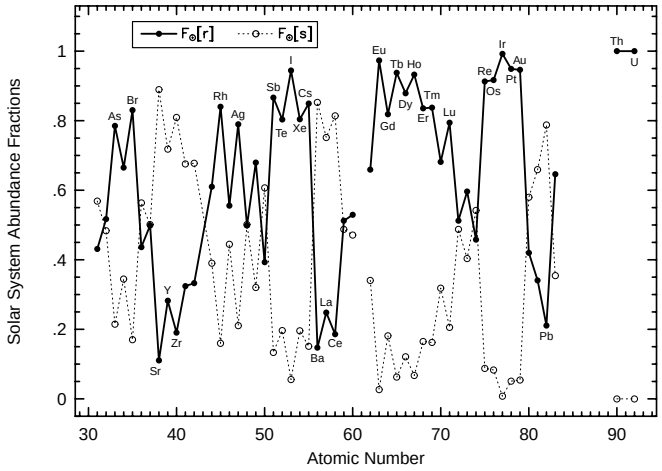

FIG. 11.—Solar system *r*- and *s*-process fractions for elemental abundances $F_\odot[r]$ and $F_\odot[s]$, computed as described in Appendix

APPENDIX

UPDATED SOLAR ELEMENTAL ABUNDANCES

Using the updated cross sections of Wisshak et al. (1996), we have recalculated the solar system *s*- and *r*-process fractions for each element. Since only a portion of the isotopes in this range have been reanalyzed by Wisshak et al., we return to Käppeler, Beer, & Wisshak (1989) for the remainder of the cross sections. Beginning with the total solar system abundances of Anders & Grevesse (1989), the individual isotopic contributions to each element were obtained from the Chart of the Nuclides. We then separated out the *s*- and *r*-process contributions to each isotope taken from either Käppeler et al. or Wisshak et al. as appropriate and summed over all the isotopes for each process. In Table 5 we list the *s*- and *r*-process elemental abundances computed in this manner. This table is similar to Table 5 in Sneden et al. (1996), with corrections to errors for Rb and Xe. In addition, we have included abundances for Lu and U, which were not included in our original table. In columns (3)–(5) we include the abundances for *r*-process, *s*-process, and total solar abundances. In columns (6) and (7) we list the fraction of total for the *r*-process ($\equiv F_\odot[r]$) and the *s*-process ($\equiv F_\odot[s]$), respectively. In Figure 11 these *r*- and *s*-process fractions are displayed so that one may easily note the dominant nucleosynthesis contribution to each element in the solar system distribution. In the figure, atomic symbols are entered near the *r*-process fractional point for those elements with solar *r*-fractions $F_\odot[r] > 0.75$ or solar system *s*-fractions $F_\odot[s] > 0.75$. Thus for example the solar system *s*-process-dominated element Ce ($F_\odot[s] = 0.8142$, Table 5) is labeled, as is the *r*-process-dominated element Ir ($F_\odot[r] = 0.9924$), but the mixed-process element Nd ($F_\odot[r] = 0.5291, F_\odot[s] = 0.4709$) is unlabeled.

REFERENCES

Anders, E., & Ebihara, M. 1982, Geochim. Cosmochim. Acta, 46, 2363
Anders, E., & Grevesse, N. 1989, Geochim. Cosmochim. Acta, 53, 197
Beers, T. C., Preston, G. W., & Shectman, S. A. 1985, AJ, 90, 2089
———. 1992, AJ, 103, 1987
Biémont, E., Grevesse, N., Hannaford, P., & Lowe, R. M. 1981, ApJ, 248, 867
Biémont, E., Karner, C., Meyer, G., Träger, F., & zu Putlitz, G. 1982, A&A, 107, 166
Biémont, E., & Lowe, R. M. 1993, A&A, 273, 665
Bond, H. E. 1980, ApJS, 44, 517
Cowan, J. J., Burris, D. L., Sneden, C., McWilliam, A., & Preston, G. W. 1995, ApJ, 439, L51
Cowan, J. J., McWilliam, A., Sneden, C., & Burris, D. L. 1997, ApJ, 480, 246
Cowan, J. J., Pfeiffer, B., Kratz, K.-L., Thielemann, F.-K., Sneden, C., Burles, S., Tytler, D., & Beers, T. C. 1999, ApJ, 521, 194
Cowan, J. J., Sneden, C., Truran, J. W., & Burris, D. L. 1996, ApJ, 460, L115
Cowan, J. J., Thielemann, F.-K., & Truran, J. W. 1991, Phys. Rep., 208, 267
Edvardsson, B., Andersen, J., Gustafsson, B., Lambert, D. L., Nissen, P. E., & Tomkin, J. 1993, A&A, 275, 101
Fitzpatrick, M. J., & Sneden, C. 1987, BAAS, 19, 1129
François, P. 1996, A&A, 313, 229
Gallagher, A. 1967, Phys. Rev., 157, 24
Gallino, R., et al. 1998, ApJ, 497, 388
Gilroy, K. K., Sneden, C., Pilachowski, C. A., & Cowan, J. J. 1988, ApJ, 327, 298
Gratton, R., & Sneden, C. 1991, A&A, 241, 501
———. 1994, A&A, 287, 927
Gustafsson, B., Bell, R. A., Ericksson, K., & Nordlund, A. 1975, A&A, 42, 407
Hannaford, P., Lowe, R. M., Grevesse, N., Biémont, E., & Whaling, W. 1982, ApJ, 261, 736
Ishimaru, Y., & Wanajo, S. 1999, ApJ, 511, L33
Jehin, E., Magain, P., Neuforge, C., Noels, A., Parmentier, G., & Thoul, A. A. 1999, A&A, 341, 241
Käppeler, F., Beer, H., & Wisshak, K. 1989, Rep. Prog. Phys., 52, 945
Kusz, J. 1992, A&AS, 92, 517
Lamb, S., Howard, W. M., Truran, J. W., & Iben, I., Jr. 1977, ApJ, 217, 213
Lattimer, J. M., Mackie, F., Ravenhall, D. G., & Schramm, D. N. 1977, ApJ, 213, 225
Magain, P. 1995, A&A, 297, 686
Maier, R. S., & Whaling, W. 1977, J. Quant. Spectrosc. Radiat. Transfer, 18, 501
Mashonkina, L., Gehren, T., & Bikmaev, I. 1999, A&A, 343, 519
Mathews, G. J., Bazan, G., & Cowan, J. J. 1992, ApJ, 391, 719
Mathews, G. J., & Cowan, J. J. 1990, Nature, 345, 491
Matteucci, F., & Greggio, L. 1986, A&A, 154, 279
McWilliam, A. 1998, AJ, 115, 1640
McWilliam, A., Preston, G. W., Sneden, C., & Searle, L. 1995a, AJ, 109, 2757
McWilliam, A., Preston, G. W., Sneden, C., & Shectman, S. 1995b, AJ, 109, 2736
Pilachowski, C. A., Sneden, C., & Booth, J. 1993, ApJ, 407, 699
Pilachowski, C. A., Sneden, C., & Kraft, R. P. 1996, AJ, 111, 1689 (PSK)
Qian, Y.-Z., Vogel, P., & Wasserburg, G. J. 1998, ApJ, 494, 285
Raiteri, C. M., Gallino, R., Busso, M., Neuberger, D., & Käppeler, F. 1993, ApJ, 419, 207
Raiteri, C. M., Villata, M., Gallino, R., Busso, M., & Cravanzola, A. 1999, ApJ, 518, L91
Rosswog, S., Liebendorfer, M., Thielemann, F.-K., Davies, M. B., Benz, W., & Piran, T. 1999, A&A, 341, 499

Ryan, S. G., Norris, J. E., & Beers, T. C. 1996, ApJ, 471, 254
Sneden, C. 1973, ApJ, 184, 839
Sneden, C., Cowan, J. J., Burris, D. L., & Truran, J. W. 1998, ApJ, 496, 235
Sneden, C., Kraft, R. P., Prosser, C. F., & Langer, G. E. 1991, AJ, 102, 2001
Sneden, C., & Parthasarathy, M. 1983, ApJ, 267, 757
Sneden, C., & Pilachowski, C. A. 1985, ApJ, 288, L55
Sneden, C., Preston, G. W., McWilliam, A., & Searle, L. 1994, ApJ, 431, L27
Sneden, C., McWilliam, A., Preston, G. W., Cowan, J. J., Burris, D. L., & Armosky, B. J. 1996, ApJ, 467, 819
Spite, M., & Spite, F. 1978, A&A, 67, 23
Travaglio, C., Galli, D., Gallino, R., Busso, M., Ferrini, F., & Straniero, O. 1999, ApJ, 521, 691
Truran, J. W. 1981, A&A, 97, 391
Wasserburg, G. J., Busso, M., & Gallino, R. 1996, ApJ, 466, L109
Ward, L., Vogel, O., Ahnesjö, A., Arnesan, A., Hallin, R., McIntyre, L., & Nordling, C. 1984, Phys. Scr., 29, 551
Ward, L., Vogel, O., Arnessan, A., Hallin, R., & Wännström, A. 1985, Phys. Scr., 31, 161
Wheeler, C., Cowan, J. J., & Hillebrandt, W. 1998, ApJ, 493, L101
Wisshak, K., Voss, F., & Käppeler, F. 1996, in Proc. 8th Workshop on Nuclear Astrophysics, ed. W. Hillebrandt, & E. Müller (Munich: MPI), 16
Woolf, V. M., Tomkin, J., & Lambert D. L. 1995, ApJ, 453, 660
Woosley, S. E., Wilson, J. R., Mathews, G. J., Hoffman, R. D., & Meyer, B. S. 1994, ApJ, 433, 229